NAVAL POSTGRADUATE SCHOOL

MONTEREY, CALIFORNIA

THESIS

HYBRID MODES IN LONG WAVELENGTH FREE ELECTRON LASERS

by

Younhoan Bae

December 2010

Thesis Co-Advisors: William B. Colson
Robert L. Armstead
Joseph Blau

Approved for public release; distribution is unlimited

THIS PAGE INTENTIONALLY LEFT BLANK

REPORT DOCUMENTATION PAGE

Form Approved OMB No. 0704-0188

1. AGENCY USE ONLY (*Leave blank*)	2. REPORT DATE	3. REPORT TYPE AND DATES COVERED
	December 2010	Master's Thesis

4. TITLE AND SUBTITLE	5. FUNDING NUMBERS
Hybrid Modes in Long Wavelength Free Electron Lasers	
6. AUTHORS Younhoan Bae	
7. PERFORMING ORGANIZATION NAME(S) AND ADDRESS(ES) Naval Postgraduate School Monterey CA 93943-5000	8. PERFORMING ORGANIZATION REPORT NUMBER
9. SPONSORING/MONITORING AGENCY NAME(S) AND ADDRESS(ES)	10. SPONSORING/MONITORING AGENCY REPORT NUMBER

11. SUPPLEMENTARY NOTES The views expressed in this thesis are those of the author and do not reflect the official policy or position of the Department of Defense or the U.S. Government. IRB Protocol Number:_____

12a. DISTRIBUTION/AVAILABILITY STATEMENT	12b. DISTRIBUTION CODE
Approved for public release; distribution is unlimited	

13. ABSTRACT(*maximum 200 words*)

Of the many Free Electron Lasers (FELs) in the world today, most are big and expensive. This is true across the wavelength spectrum, from long to very short. In contrast, the FEL facility in progress at NPS, which will initially operate at long wavelengths and at electron energies of only a few MeV, is inexpensive and smaller. However, longer wavelengths lead to more diffraction, which may result in beam spread and interaction with the undulator surfaces. Anticipating the possibility, in this thesis we analyze mathematically the free space Hermite-Gaussian modes of the optical beam, and then compare them to the Hybrid modes, where waveguide plates control diffraction along one axis, allowing free space diffraction along the other axis. We continue the analysis of the relativistic electron beam, co-propagating with the optical wave in the Hybrid Mode, to define new operating condition for the FEL.

14. SUBJECT TERMS Free Electron Laser, Resonator Modes, Hermite-Gaussian Modes, Hybrid(HG-Waveguide) Modes	15. NUMBER OF PAGES 81
	16. PRICE CODE

17. SECURITY CLASSIFICATION OF REPORT	18. SECURITY CLASSIFICATION OF THIS PAGE	19. SECURITY CLASSIFICATION OF ABSTRACT	20. LIMITATION OF ABSTRACT
Unclassified	Unclassified	Unclassified	UU

NSN 7540-01-280-5500

Standard Form 298 (Rev. 2-89)
Prescribed by ANSI Std. 239-18 298-102

THIS PAGE INTENTIONALLY LEFT BLANK

Approved for public release; distribution is unlimited

HYBRID MODES IN LONG WAVELENGTH FREE ELECTRON LASERS

Younhoan Bae
Captain, Republic Of Korea Army
B.S., Korea Military Academy, 2006

Submitted in partial fulfillment of the
requirements for the degree of

MASTER OF SCIENCE IN APPLIED PYHSICS

from the

NAVAL POSTGRADUATE SCHOOL
December 2010

Author: Younhoan Bae

Approved by: William B. Colson
Thesis Co-Advisor

Robert L. Armstead
Thesis Co-Advisor

Joseph Blau
Thesis Co-Advisor

Andres Larraza
Chairman, Department of Physics

THIS PAGE INTENTIONALLY LEFT BLANK

ABSTRACT

Of the many Free Electron Lasers (FELs) in the world today, most are big and expensive. This is true across the wavelength spectrum, from long to very short. In contrast, the FEL facility in progress at NPS, which will initially operate at long wavelengths and at electron energies of only a few MeV, is inexpensive and smaller. However, longer wavelengths lead to more diffraction, which may result in beam spread and interaction with the undulator surfaces. Anticipating the possibility, in this thesis we analyze mathematically the free space Hermite-Gaussian modes of the optical beam, and then compare them to the Hybrid modes, where waveguide plates control diffraction along one axis, allowing free space diffraction along the other axis. We continue the analysis of the relativistic electron beam, co-propagating with the optical wave in the Hybrid Mode, to define new operating condition for the FEL.

THIS PAGE INTENTIONALLY LEFT BLANK

DISCLAIMER

This thesis was typed using LaTeX2ε on an Apple iMac. For information on LaTeX, or the code used for this thesis, please feel free to contact me at my permanent e-mail address: qo1504@nate.com.

THIS PAGE INTENTIONALLY LEFT BLANK

TABLE OF CONTENTS

LIST OF FIGURES

THIS PAGE INTENTIONALLY LEFT BLANK

LIST OF TABLES

THIS PAGE INTENTIONALLY LEFT BLANK

ACKNOWLEDGMENTS

I would like to first thank the Republic of Korea Army for giving me this opportunity to obtain a master's degree here at the Naval Postgraduate School. Secondly, I also would like to thank all who helped me in this process: professors Bill Colson, Bob Armstead, and Joseph Blau, and Dr. Sean Niles, who graduated September 2010. Finally, I want to extend a thank to my wife, Yujin Lee, for her support over a year.

THIS PAGE INTENTIONALLY LEFT BLANK

I. INTRODUCTION

The Free Electron Laser (FEL) uses a beam of relativistic electrons co-propagating with an optical beam in a periodic magnetic field. This magnetic field causes the free electrons to oscillate, allowing coherent energy exchange between the electron beam and the optical beam.

The first development relevant to the FEL was the microwave tube, invented in the 1930s, which utilized a beam of free nonrelativistic electrons in a closed microwave cavity. Later, atomic and molecular lasers that employed a system of bound electrons and an open optical resonator were devised in the 1960s. By using a beam of free relativistic electrons and the open optical resonator, J. M. J. Madey, the inventor of the FEL, combined the attributes of microwave tubes of the 1930s and the atomic lasers of the 1960s [1].

Today there are many FELs to be found in the world, and most of these produce high quality laser light at IR wavelengths for scientific research. FELs generating short wavelengths, UV and X-ray, have been studied extensively during the past four decades; these require large and expensive accelerators with electron energy on the order of GeV. In this thesis, I will focus on long wavelength FELs, which require only a few MeV for the electron beam energy and much simpler technology with lower costs. This thesis work will provide a basic theory for designing FELs to operate at long wavelengths in the laboratory. Since NPS is starting a FEL facility that will first reach lower energies of only a few MeV, the FEL considered here could be the first to operate at NPS.

The thesis is organized as follows: Chapter II describes the FEL system, briefly discussing how FELs work and their significant attributes. Chapter III describes the basic theory of FEL operation dealing with the electron behavior and interaction between the electron beam and the optical field. This chapter will be limited to plane waves to characterize the optical field. However, FELs actually operate in

Gaussian wave modes. So Chapter IV offers the solution of the wave equation, with an emphasis on Hermite Gaussian resonator modes. Then Chapter V explores FEL theory, including the features of Hermite Gaussian resonator modes. Chapter VI deals with Hybrid (HG-Waveguide) resonator modes. These are important to analyze, because in order to operate a FEL at long wavelengths, we may need to use waveguide structure capable of confining the radiation that otherwise spreads due to diffraction. New research is then presented in Chapter VII to suggest an FEL theory applied to Hybrid (HG-Waveguide) resonator modes, which is the ultimate goal of this thesis.

II. FREE ELECTRON LASER SYSTEM DESCRIPTION

The Free Electron Laser system consists of several different elements involving interesting physics. Figure 1 shows the major components of an FEL system such as the Jefferson Lab 14kW IR FEL, and the proposed NPS FEL. There are two basic configurations of an FEL, the oscillator and the amplifier, which will be examined in the following section. Most of the components shown in Figure 1 are common to both designs.

A pulsed electron beam is produced when an injector sends the beam into an accelerator, such as superconducting linear accelerator. The beam of electrons is accelerated to near the speed of light utilizing radio-frequency (RF) fields. The relativistic electrons enter the undulator and then get "wiggled" to produce laser light, bringing about coherent emission. In this process, only a small fraction (typically $\sim$ 1–2%) of the electron beam energy is converted to optical energy. In some cases, the electrons are then re-circulated through the accelerator in order to recover most of their remaining energy. Finally, the electron beam enters the beam dump.

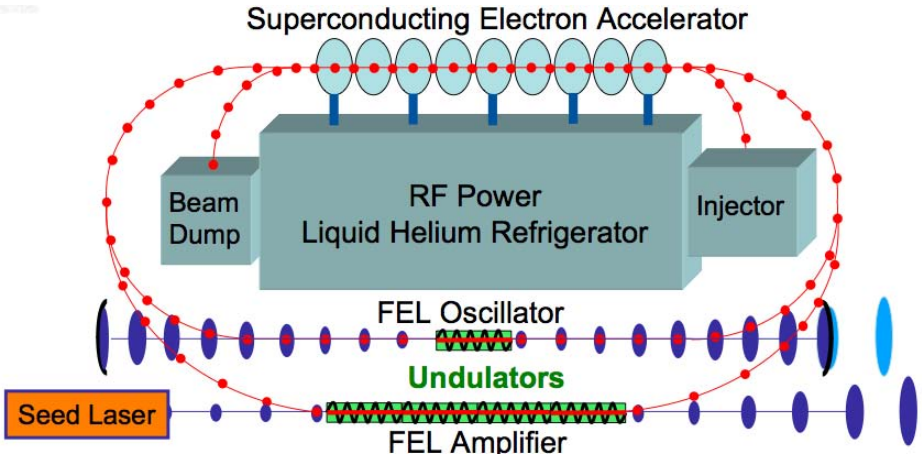

Figure 1. FEL main system schematic. Note the two configurations identified as the "Oscillator" or the "Amplifier." Red dots represent the electron pulses, and blue ellipses describe the optical pulses. From [2].

A. CONFIGURATIONS

In an oscillator configuration, the radiation is stored and amplified between two reflective mirrors as shown in Figure 2. The optical beam is then outcoupled through a partially transmitting mirror. Coherence is developed through many passes of the optical field through the undulator.

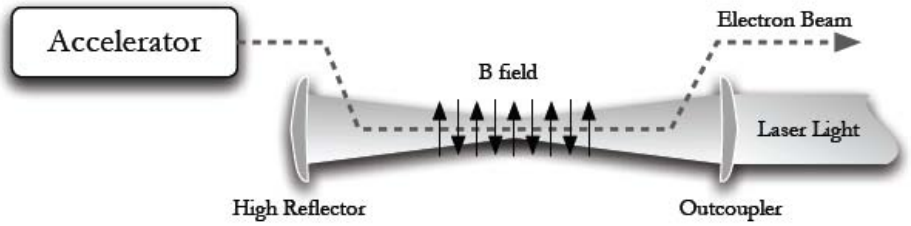

Figure 2. FEL schematic in an oscillator configuration. From [3].

In an amplifier configuration, the optical resonator does not exist; instead, the system employs a "seed laser," which is an external laser source. Since only one pass is used, the amplifier uses a longer undulator to attain more gain. Coherence in this case is established by the seed laser. Figure 3 shows a typical amplifier configuration.

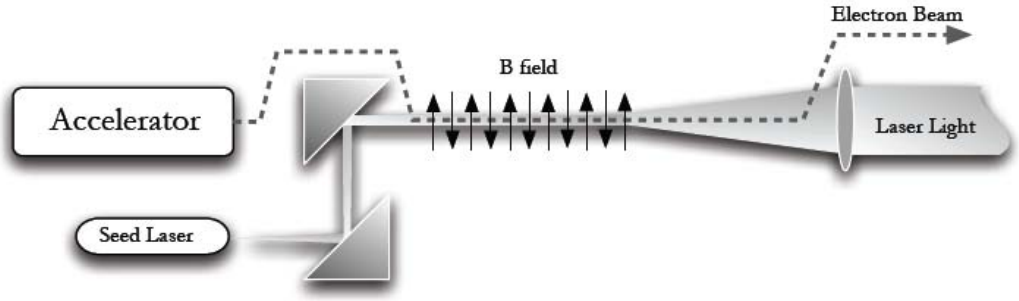

Figure 3. FEL schematic in an amplifier configuration. From [3].

B. ATTRIBUTES

The FEL has some unique attributes such as tunability, designability, high power, efficiency and reliability. Tunability separates the FEL from a conventional

laser in which the wavelength is determined by atomic energy levels. n an FEL, the resonance condition between the Lorentz factor γ of the electron beam, the undulator period λ_0, and the dimensionless undulator parameter K determine the laser wavelength λ:

$$\lambda = \frac{\lambda_0 \left(1 + K^2\right)}{2\gamma^2}, \tag{II.1}$$

where K is proportional to the magnetic field of the undulator. This relationship means that by changing the spacing of the magnets, the strength of the magnetic field, or the energy of the electron beam, the FEL can be continuously tuned to different wavelengths. Also, FELs have been designed over a wide range of wavelengths, from microwaves to X-rays; that is, they possess "designability." The absence of a vulnerable medium such as gasses, fluid chemicals or solid materials means that the FEL has the potential to achieve extremely high power. As a result, the FEL can have good efficiency ($\sim 10\%$) when recirculating the electron beam. The final advantage of the FEL is reliability: existing FEL systems now run twenty-four hours a day for weeks. On the down side, the FEL is as huge as a laboratory and considerably expensive.

C. COMPONENTS

The major components of an FEL system are an injector, an accelerator, an undulator, a resonator for the oscillator, a seed laser for the amplifier, and a beam dump. There are many other constituents that allow the FEL to operate, such as bending magnets for steering the path of the electron beam, an optical beam transport system, radiation shielding and vibration control.

1. Injector

The injector generates and accelerates the beam of free electrons to about ~ 5 MeV energy. There are several ways to produce the beam of free electrons. Typically, the free electrons are emitted into vacuum through either thermionic emission or the photoelectric effect. In the thermionic cathode, the electrons are emitted from the

surface of the cathode when the cathode is heated sufficiently. A photocathode uses an incident drive laser to excite the electrons in a cathode. By using the photoelectric effect, electrons are ejected as long as the photon energy is greater than the cathode work function. The released electrons can be emitted into a Radio Frequency (RF) cavity, that accelerates the electrons to the desired energies ($\sim$ 5 MeV) before they enter the main accelerator. The electron beams usually come out in pulses with excellent quality (a narrow, collimated beam with low energy spread); not maintaining such beam quality can affect FEL system performance. An RF injector is shown in Figure 4.

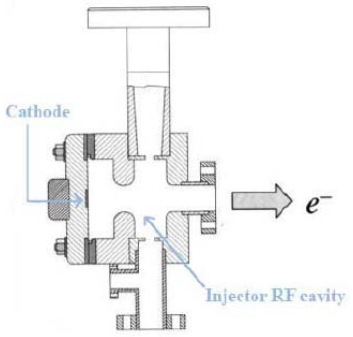

Figure 4. Schematic of an injector. From [4].

2. Accelerator

After the injector, the electron beam is now passed on to the accelerator. The accelerator increases the energy of the electron beam from $\sim$ 5 MeV to the desired level. Direct Current (DC) acceleration is possible, but most FELs use a Radio Frequency Linear Accelerator (RF LINAC) to obtain a final energy of $\sim$ 100 MeV. The accelerator may consist of several evacuated superconducting metal RF cavities. The electromagnetic field generated in each cavity should be in phase with the injected electron pulses to provide net positive acceleration.

3. Undulator

The undulator is a significant part of the FEL located inside the optical resonator cavity and typically consists of alternating permanent magnets. When the electrons leave the accelerator, they enter the periodic magnetic field and are made to wiggle in a transverse direction by the Lorentz force. The wiggling motion causes the electrons to radiate photons and amplify the light already in the undulator. As the electrons and light interact in the undulator, there is an exchange of energy: some electrons gain energy from the light and some lose energy to the light. The electrons that gain energy move a little bit faster along the axis of the undulator and those that lose energy move a little bit slower; this causes "micro bunching" of the electrons on the scale of an optical wavelength. Undulators typically have either linear or helical polarization. A linear undulator drives the electrons to move sinusoidally in a plane while, a helical undulator drives them to a corkscrew motion. A schematic of an undulator and the electron beam path is shown in Figure 5.

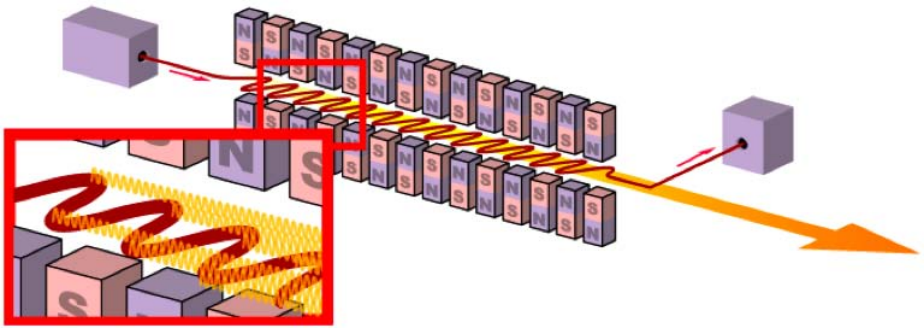

Figure 5. Schematic of an undulator. The red line is the electron beam wiggling along the transverse axis. The yellow lines indicate the stimulated emission propagating along an axis of forward direction. The undulator consists of magnets alternating north and south poles, resulting in the periodic magnetic fields. From [5].

4. Resonator

In the oscillator configuration, the resonator is the component in which the light is stored and amplified over many passes. It is made up of an evacuated cavity bounded by two mirrors. One of the mirrors has high reflectivity, while the other allows a percentage to come out through a partially-transmitting mirror. The light derived from this out-coupling mirror is the usable laser light of the FEL system. It is obvious that for maximum coupling efficiency, electron pulses must be synchronized with the bounce time of optical pulses between resonator mirrors. A schematic of the electron and optical pulses passing through the undulator in the resonator is shown in Figure 6.

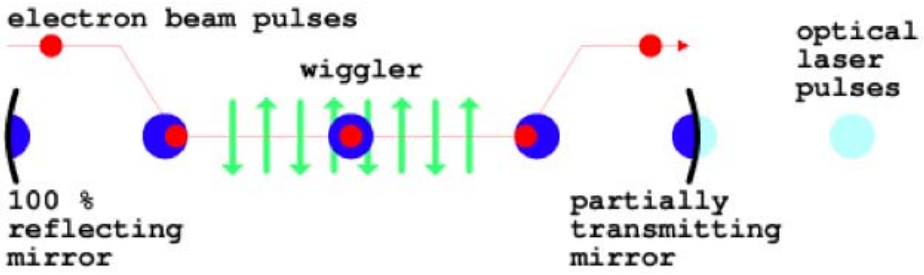

Figure 6. Schematic of a resonator. From [2].

5. Beam Dump

The beam dump is the last part of the electron beam path. It consists of an absorbing material (such as a large metal block) surrounded by radiation shielding. Extracting energy from the electron beam amplifies the optical beam, but the extraction of energy is typically only a few percent, leaving a high-energy electron beam which results in poor system efficiency, and lots of potentially dangerous radiation emitted at the dump. If the system uses recirculation of the electron beam, the electrons enter to the LINAC a second time 180 ° out of phase, decelerating electrons, and giving most of their energy back to the RF field. The recirculated electron beam has approximately ∼3 MeV average energy at the end of the LINAC, having lost a

few percent to the laser beam and leaving about the same energy that the electron beam had when it was generated at the injector. This greatly improves overall system efficiency, and reduces radiation shielding requirements at the dump. A schematic of a beam dump is shown in Figure 7.

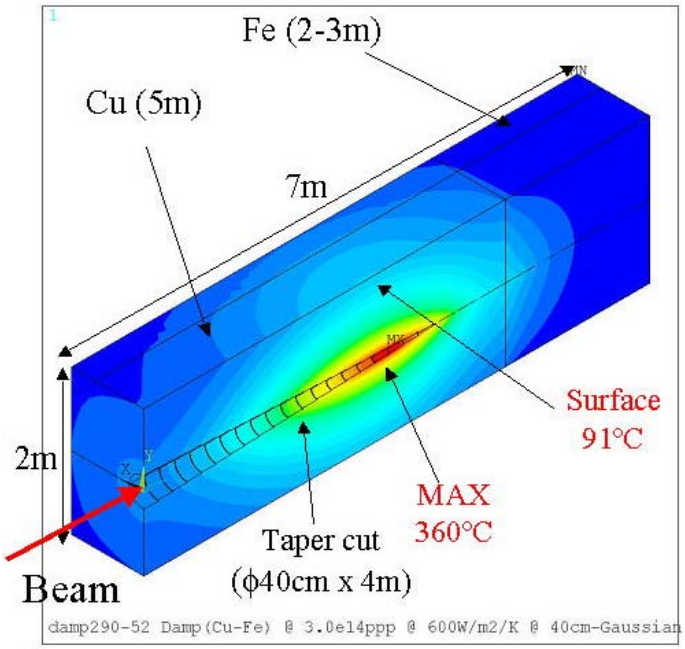

Figure 7. Schematic of a beam dump. From [7].

THIS PAGE INTENTIONALLY LEFT BLANK

III. BASIC FREE ELECTRON LASER THEORY

We will now explore the mathematics that describe the operation of the FEL. The physics of the electron's behavior and the interaction between the electron beam and optical field are pivotal to the operation of FEL systems. In the following sections, the x and y-axis designate the transverse axes while the z-axis designates the longitudinal axis passing through the center of the undulator.

A. ELECTRON BEHAVIOR

The electrons in the undulator have a microscopic evolution.

1. Undulator Field and Transverse Motion

Exploring the behavior of electrons in the magnetic field of the undulator is necessary to understand the physics of the FEL interaction. We will deal with relativistic electrons entering a helical undulator field (which is simpler mathematically than a linear undulator) in helical orbits around the z-axis in the presence of the optical field. An electron passing through the undulator is exposed to three fields: the magnetic field from the undulator magnets, the magnetic field of the optical wave and the electric field of the optical wave, as shown in Figure 8.

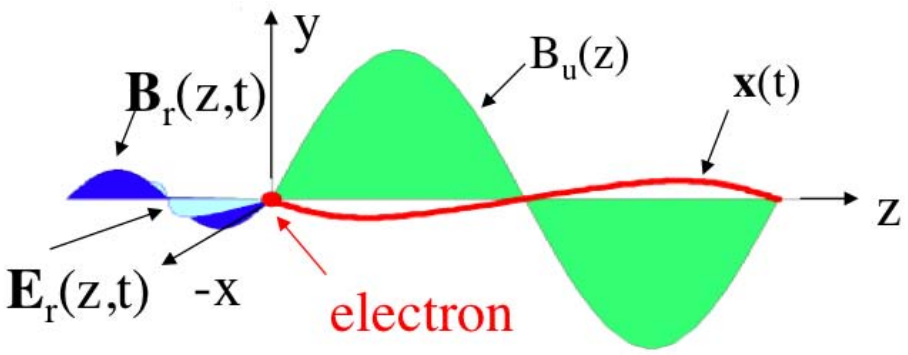

Figure 8. For convenience, undulator and Optical Fields in the case of linear undulator. From [2]

The magnetic field of the helical undulator is

$$\mathbf{B}_u = B\left[\cos\left(k_0 z\right), \sin\left(k_0 z\right), 0\right] \tag{III.1}$$

where B is the magnetic field amplitude, $k_0 = 2\pi/\lambda_0$ is the undulator wave number and λ_0 is the undulator's period which is the distance of one complete cycle of the magnetic field in the undulator. The corresponding electric and magnetic field of the optical field are

$$\mathbf{E}_r = E\left(\cos\psi, -\sin\psi, 0\right) \tag{III.2}$$

$$\mathbf{B}_r = E\left(\sin\psi, \cos\psi, 0\right) \tag{III.3}$$

where E is the optical wave amplitude in cgs units, $\psi = kz - wt + \phi$, $k = 2\pi/\lambda$ is the optical wave number, $w = kc$ is the optical angular frequency, and ϕ is the optical phase.

The relativistic Lorentz force equations determine the electron motion in the undulator. The relativistic Lorentz force equations in cgs units [1] for an electron are

$$\frac{\mathrm{d}}{\mathrm{d}t}\left(\gamma\boldsymbol{\beta}\right) = -\frac{e}{mc}\left[\mathbf{E_r} + \boldsymbol{\beta}\times\left(\mathbf{B_u} + \mathbf{B_r}\right)\right], \tag{III.4}$$

$$\frac{\mathrm{d}\gamma}{\mathrm{d}t} = -\frac{e}{mc}\boldsymbol{\beta}\cdot\mathbf{E_r}, \tag{III.5}$$

$$\gamma^{-2} = 1 - \boldsymbol{\beta}\cdot\boldsymbol{\beta}, \tag{III.6}$$

where $\mathbf{v} = \boldsymbol{\beta}c$ is the electron velocity, $e = \mid e \mid$ is the electron change magnitude, m is the electron mass, c is the speed of the light, and γ is the relativistic Lorentz factor. Substituting the fields from Equations (III.1), (III.2), and (III.3) into the (III.4), we get

$$\frac{\mathrm{d}}{\mathrm{d}t}\left(\gamma\beta_x\right) = -\frac{e}{mc}\left[E\cos\psi\left(1-\beta_z\right) - \beta_z B\sin\left(k_0 z\right)\right], \tag{III.7}$$

$$\frac{\mathrm{d}}{\mathrm{d}t}\left(\gamma\beta_y\right) = -\frac{e}{mc}\left[-E\sin\psi\left(1-\beta_z\right) + \beta_z B\cos\left(k_0 z\right)\right], \tag{III.8}$$

$$\frac{\mathrm{d}}{\mathrm{d}t}\left(\gamma\beta_z\right) = -\frac{e}{mc}\left[E\left(\beta_x\cos\psi - \beta_y\sin\psi\right) + B\{\beta_x\sin\left(k_0 z\right) - \beta_y\cos\left(k_0 z\right)\}\right]. \tag{III.9}$$

Since the electrons are traveling close to the speed of light along the z axis, $\beta_z \approx 1$, so that terms containing $(1-\beta_z)$ can be ignored in the transverse x-y components of Equations (III.7) and (III.8). In other words, $E(1-\beta_z)$ is small compared to $\beta_z B$, which means magnetic fields derived from an undulator have a bigger effect on the electron's transverse motion than the optical fields. Integrating Equations (III.7) and (III.8) with respect to time and setting the constant of integration to zero, indicating perfect injection into helical orbits, we get

$$\beta_x = -\frac{K}{\gamma}\cos(k_0 z), \tag{III.10}$$

$$\beta_y = -\frac{K}{\gamma}\sin(k_0 z), \tag{III.11}$$

where $K = eB_{rms}\lambda_0/2\pi mc^2$ is the dimensionless undulator parameter and B_{rms} is the rms value of the undulator field. For the helical undulator $B_{rms} = B$; for the linearly polarized undulator $B_{rms} = B/\sqrt{2}$. Integrating once again and using $k_0 z = k_0 v_z t = k_0 \beta_z ct \approx k_0 ct = \omega_0 t$, we get

$$x(t) = -\frac{cK}{\omega_0\gamma}\sin(\omega_0 t) = -\frac{K\lambda_0}{2\pi\gamma}\sin(\omega_0 t), \tag{III.12}$$

$$y(t) = -\frac{cK}{\omega_0\gamma}\cos(\omega_0 t) = -\frac{K\lambda_0}{2\pi\gamma}\cos(\omega_0 t), \tag{III.13}$$

which describes the transverse (helical) motion of the electron.

2. Longitudinal Motion and the Electron Phase

Now consider the effects of the optical electric field. We scrutinize the microscopic electron motion along the longitudinal axis which, while small in magnitude, is key to FEL operation. Substituting Equations (III.10) and (III.11) into (III.9) and using a trigonometric identity gives

$$\gamma\dot{\beta}_z = \frac{eKE}{\gamma mc}\cos(k_0 z + \psi) - \dot{\gamma}\beta_z. \tag{III.14}$$

In order to get $\dot{\gamma}$, substitute Equations (III.10), (III.11) and (III.2) into (III.5) and get

$$\frac{\mathrm{d}\gamma}{\mathrm{d}t} = \dot{\gamma} = \frac{eKE}{\gamma mc}\cos(k_0 z + \psi). \tag{III.15}$$

Substituting Equation (III.15) into (III.14), we arrive at

$$\dot{\beta}_z = (1 - \beta_z) \frac{eKE}{\gamma^2 mc} \cos(k_0 z + \psi). \tag{III.16}$$

Also, we can rewrite the Equation (III.15) by using the definition of ψ and the "electron phase," $\zeta = (k + k_0) z - \omega t$, which describes the electron's phase with respect to the combined optical and undulator fields, to obtain

$$\dot{\gamma} = \frac{eKE}{\gamma mc} \cos(\zeta + \phi). \tag{III.17}$$

Since k_0, k and ω are fixed, the dynamical variable in $\zeta(t)$ is $z(t)$ which represents the electron's microscopic position, $\zeta \propto kz(t)$. Note that when $\cos(\zeta + \phi) > 0$, the electron energy increases by absorption, $\dot{\gamma} > 0$; when $\cos(\zeta + \phi) < 0$, the electron energy decreases by stimulated emission, $\dot{\gamma} < 0$. This causes the electron beam to bunch and to radiate coherently.

3. Resonance Condition and Pendulum Equation

FEL resonance occurs when the energy exchange between the electron and the optical beam is optimum. The electron travels down the z-axis with a speed $\beta_z c$ while the optical pulse travels at the speed of light, c. The relationship between these two speeds brings about the "electron-photon race," which is illustrated in Figure 9.

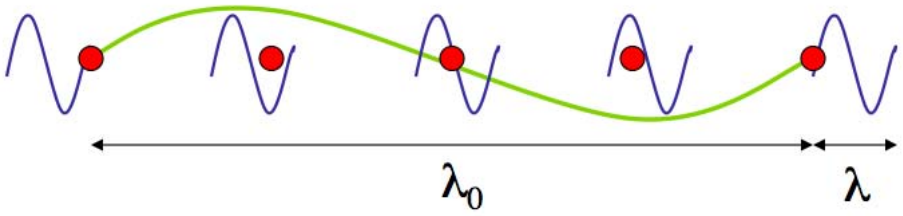

Figure 9. Electron-photon race. From [2].

The time for an electron to travel through one undulator period is $\lambda_0/\beta_z c$. During that time, one wavelength of light is emitted because the electron executes one oscillation in the undulator. The wavelength of light then travels a distance $\lambda + \lambda_0$ at speed c.

So,

$$\frac{\lambda_0}{\beta_z c} = \frac{\lambda + \lambda_0}{c}. \tag{III.18}$$

From (III.18) we see that the laser wavelength at resonance is

$$\lambda = \frac{\lambda_0 \left(1 - \beta_z\right)}{\beta_z}. \tag{III.19}$$

Now we find an expression for β_z in terms of the dimensionless undulator parameter, K. From Equations (III.10) and (III.11), we find that ${\beta_\perp}^2 = K^2/\gamma^2$. Therefore, the relativistic Lorentz factor, γ, which indicates the relationship between the electron energy γmc^2 and the z-axis velocity $c\beta_z$ can be expressed as

$$\gamma^{-2} = 1 - \boldsymbol{\beta}^2 = 1 - {\boldsymbol{\beta}_\perp}^2 - {\beta_z}^2 = 1 - \frac{K^2}{\gamma^2} - {\beta_z}^2. \tag{III.20}$$

For relativistic electrons, $\gamma \gg 1$, we can use the binomial expansion to get

$$\beta_z \approx 1 - \frac{1 + K^2}{2\gamma^2}. \tag{III.21}$$

We can rewrite the resonance condition, Equation (III.9), in terms of K to get

$$\lambda \approx \frac{\lambda_0 \left(1 + K^2\right)}{2\gamma^2}. \tag{III.22}$$

By changing the physical parameters, such as λ_0, K and γ, we can get a wide range of wavelengths of the optical beam, which indicates the FEL's tunability. Also we can now see that the wavelength of the optical beam λ is much smaller than the undulator period λ_0 because of the small factor $1/\gamma^2$.

Now we are ready to derive the FEL"pendulum equation" by combining some of the previous equations. Let us introduce an operator $\overset{\circ}{(..)} = \mathrm{d}\left(..\right) / \mathrm{d}\tau$ which can be expressed as

$$\frac{\mathrm{d}}{\mathrm{d}\tau} = \frac{\mathrm{d}}{\mathrm{d}t}\frac{\mathrm{d}t}{\mathrm{d}\tau} = \frac{L}{c}\frac{\mathrm{d}}{\mathrm{d}t},$$

where $\tau \equiv ct/L$ is the "dimensionless time," where L is the undulator length, so that $\tau = 0 \rightarrow 1$ along the undulator. By using this relation, we can determine the rate of change of the electron phase along the undulator as the electron phase velocity,

$$\nu \equiv \frac{\mathrm{d}\zeta}{\mathrm{d}\tau} = \overset{\circ}{\zeta} = L\left[\left(k + k_0\right)\beta_z - k\right], \tag{III.23}$$

where the derivative of ζ(electron phase) is with respect to τ; again $L = N\lambda_0$ is the length of the undulator, so that $0 \leq \tau \leq 1$. By substituting Equation (III.21) into (III.23) and using $k \gg k_0$ near resonance, we arrive at [6]

$$\mathrm{d}\nu = 4\pi N \frac{\mathrm{d}\gamma}{\gamma}, \tag{III.24}$$

relating changes in beam energy to the electron phase velocity. Combining Equation (III.15) and (III.24) gives

$$\frac{\mathrm{d}\nu}{\mathrm{d}\tau} = \frac{L}{c}\frac{\mathrm{d}\nu}{\mathrm{d}t} = \frac{L}{c}\frac{\mathrm{d}\nu}{\mathrm{d}\gamma}\frac{\mathrm{d}\gamma}{\mathrm{d}t} = \frac{L}{c}\frac{4\pi N}{\gamma}\frac{eKE}{\gamma mc}\cos\left(\zeta + \phi\right),$$

$$\mathring{\nu} = \mathring{\zeta} = \mid a \mid \cos\left(\zeta + \phi\right), \tag{III.25}$$

where $\mid a \mid = 4\pi NeKLE/\gamma^2 mc^2$ is the "dimensionless optical field amplitude." Equation (III.25) has the form of the pendulum equation, and describes the microscopic motion of the electrons in phase space, (ζ, ν).

4. Phase Space Evolution

Since phase velocity is associated with the electron energy according to Equation (III.24), phase space diagrams show an energy exchange between electrons and the optical field. Assuming $\mid a \mid$ and ϕ are approximately constant, the electrons follow phase space paths given by [8]

$$\nu^2 = {\nu_0}^2 + 2 \mid a \mid \left[\sin\left(\zeta + \phi\right) - \sin\left(\zeta_0 + \phi\right)\right], \tag{III.26}$$

where ζ_0 and ν_0 are the initial electron coordinates in phase space. A special phase space path is the FEL separatrix [9], starting at the unstable fixed point ($\zeta_0 = 3\pi/2$ and $\nu_0 = 0$), so that

$$\nu^2 = 2 \mid a \mid \left[1 + \sin\left(\zeta + \phi\right)\right]. \tag{III.27}$$

From this equation, we can see that the peak to peak height of the separatrix is $4\mid a \mid^{1/2}$. A larger $\mid a \mid$ results in the phase space paths evolving much faster and a separatrix increased in height. Inside the separatrix, the electrons follow closed orbits (corresponding to a pendulum swinging back and forth). Outside the separatrix, the

electrons follow open orbits (like a pendulum swinging over the top). Figure 10 shows the evolution of 20 sample electrons at resonance $\nu_0 = 0$ and weak field $a_0 < \pi$ during the dimensionless time from $\tau = 0$ (yellow dots) to $\tau = 1$(red dots).

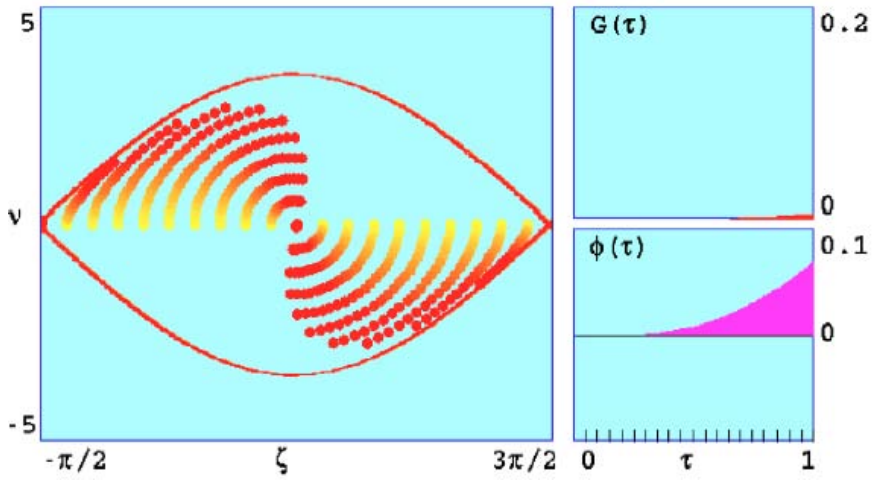

Figure 10. Phase space evolution of electrons injected at resonance ($\nu_0 = 0$), and corresponding optical field gain and phase evolution. From [4].

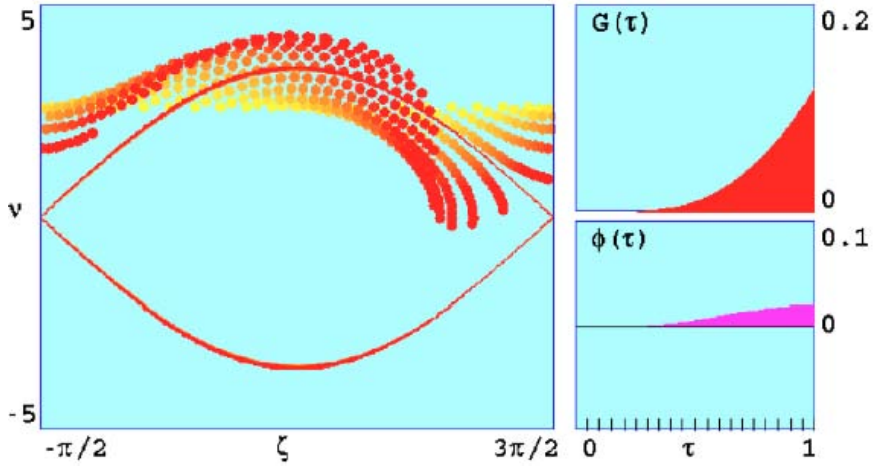

Figure 11. Phase space evolution of electrons injected off resonance ($\nu_0 = 2.6$), and corresponding optical field gain and phase evolution. Periodic boundary conditions are applied to keep the electron phase ζ between $-\pi/2$ and $3\pi/2$. From [4].

The symmetrical distributions of the electrons indicates that about half of the electrons gain energy from the optical field (paths shift up) and, the other half lose energy

to the optical field (paths shift down). We can see a bunching of electrons occurs but there is no gain since an equal number of electrons gained and lost energy.

If electrons were injected slightly off resonance ($\nu_0 = 2.6$), as shown in Figure 11, more electrons would shift to a lower value of phase velocity than shift to higher energy. There is an obvious bunching of electrons near $\zeta = \pi$, which causes the positive gain.

Gain is the ratio of the change to the initial value in the power of the optical field as it passes along the undulator. We can express the gain as

$$G(\tau) = \frac{a^2(\tau) - {a_0}^2}{{a_0}^2}, \tag{III.28}$$

where $a(\tau)$ is the field along the undulator at τ and a_0 is the initial field starting at beginning of the undulator.

B. ELECTRON-OPTICAL FIELD INTERACTION

We derived the pendulum equation which represents the microscopic evolution of the electrons in the FEL interaction region. We now need to derive an equation describing the self-consistently evolving optical field.

1. Maxwell's Equations

Now, consider the interaction between the electron beam and optical field, and start with Maxwell's equations in *cgs* units [10]:

$$\begin{aligned} \nabla \cdot \mathbf{E} &= 4\pi\rho \\ \nabla \cdot \mathbf{B} &= 0 \\ \nabla \times \mathbf{E} &= -\frac{1}{c}\frac{\partial \mathbf{B}}{\partial t} \\ \nabla \times \mathbf{B} &= \frac{4\pi}{c}\mathbf{J} + \frac{1}{c}\frac{\partial \mathbf{B}}{\partial t}, \end{aligned} \tag{III.29}$$

where ρ is the charge density, $\mathbf{J}$ is the current density. From Maxwell's equations, we can derive the full wave equation associated with transverse current [8],

$$\left(\nabla^2 - \frac{1}{c^2}\frac{\partial^2}{\partial t^2}\right)\mathbf{A}(\mathbf{x}, t) = -\frac{4\pi}{c}\mathbf{J}_\perp(\mathbf{x}, t), \tag{III.30}$$

where $\mathbf{A}(\mathbf{x},t)$ is the optical vector potential, c is the speed of light, and $\mathbf{J}_\perp(\mathbf{x},t)$ is the transverse current density; in our case, due to the wiggling motion of the electrons traveling through the undulator.

2. FEL Wave Equation

For our helical undulator, the optical vector potential can be written as

$$\mathbf{A}(\mathbf{x},t) = \frac{E(\mathbf{x},t)}{k}\hat{\varepsilon}e^{i\alpha}, \tag{III.31}$$

where $E = \mid E \mid e^{i\phi}$ is the complex laser electric field, $\alpha = kz - \omega t$ is the carrier wave, $\hat{\varepsilon} = (-i, 1, 0)$ is the laser field's polarization vector for the case of circular polarization from a helical undulator, and $\mathbf{x} = x\hat{i} + y\hat{j} + z\hat{k}$ is the position vector. By substituting Equation (III. 31) into (III. 30) and assuming that the optical wave amplitude $\mid E(\mathbf{x},t) \mid$ and phase $\phi(\mathbf{x},t)$ are slowly varying along the z axis, we arrive at [2]

$$\left[\nabla_\perp{}^2 + 2ik\left(\frac{\partial}{\partial z} + \frac{1}{c}\frac{\partial}{\partial t}\right)\right] E = -\frac{4\pi k}{c}\mathbf{J}_\perp \cdot \hat{\varepsilon}^* e^{-i\alpha}, \tag{III.32}$$

which is the parabolic or paraxial wave equation with a source current $\mathbf{J}_\perp$. When we change the variables to a reference frame that "follows the light," $u = z - L\tau = z - ct$ and $\tau = ct/L$, then we can rewrite the operator [11]

$$\frac{\partial}{\partial z} + \frac{1}{c}\frac{\partial}{\partial t} = \frac{1}{L}\frac{\partial}{\partial \tau}. \tag{III.33}$$

The source current $\mathbf{J}_\perp$ which is the sum of all single-particle currents can be expressed as

$$\mathbf{J}_\perp = -ec\sum_i \boldsymbol{\beta}_\perp \delta^{(3)}(\mathbf{x} - \mathbf{x}_i(t)), \tag{III.34}$$

where $\delta^{(3)}(\mathbf{x} - \mathbf{x}_i(t)) = \delta(x)\delta(y)\delta(z)$ is the three-dimensional Dirac delta function, and $\mathbf{x}_i(t)$ is the i^{th} electron position at time t. The transverse motion of an electron $\boldsymbol{\beta}_\perp$ which contributes to the transverse current $\mathbf{J}_\perp$ in the undulator can be expressed as

$$\boldsymbol{\beta}_\perp = -\frac{K}{\gamma}\left(\cos k_0 z, \sin k_0 z, 0\right) = \mathrm{Re}\left(-\frac{K}{\gamma} i\hat{\varepsilon} e^{-ik_0 z}\right). \tag{III.35}$$

Substituting Equation (III. 35) into (III. 34), and (III. 34) into (III. 32) gives

$$\left[\nabla_\perp{}^2 + \frac{2ik}{L}\frac{\partial}{\partial\tau}\right] E(\mathbf{r},\tau) = -4\pi ieKk\rho(\mathbf{x},t)\left\langle e^{-i\zeta}/\gamma\right\rangle, \tag{III.36}$$

where $\mathbf{r} = x\hat{i}+y\hat{j}$, and $\rho(\mathbf{x},t) = \int\sum_i \delta^{(3)}\left(\mathbf{x}-\mathbf{x}_i(t)\right)dV$ is the local electron density in a small volume element dV, and $< ... >$ indicates an average over sample electrons in the volume element. If we multiply Equation (III. 36) by $(4\pi NeKL/\gamma^2mc^2)(-Li/2k)$ and define the complex laser field $a =\mid a \mid e^{i\phi}$ with the previous laser field amplitude $\mid a \mid = 4\pi NeKLE/\gamma^2mc^2$, we can get

$$\left[-\frac{iL}{2k}\nabla_\perp{}^2 + \frac{\partial}{\partial\tau}\right] a(\mathbf{r},\tau) = -\left\langle je^{-i\zeta}\right\rangle, \tag{III.37}$$

where $j = 8N(e\pi KL)^2\rho/\gamma^3mc^2$ is the "dimensionless current density" which represents another important FEL parameter (maybe the most important). By introducing the dimensionless transverse coordinates $\tilde{x} = x\,(k/2L)^{1/2}$, $\tilde{y} = y\,(k/2L)^{1/2}$ and replacing the Laplacian operator with a dimensionless Laplacian operator, $\nabla_\perp{}^2 = (k/2L)\widetilde{\nabla}_\perp^2$, we arrive at the FEL wave equation [11]

$$\left[-\frac{i}{4}\widetilde{\nabla}_\perp^2 + \frac{\partial}{\partial\tau}\right] a(\mathbf{r},\tau) = -\left\langle je^{-i\zeta}\right\rangle, \tag{III.38}$$

where $\widetilde{\nabla}_\perp^2 = \partial_{\tilde{x}}{}^2 + \partial_{\tilde{y}}{}^2$, and the coordinates (x,y,z,τ) are all now dimensionless. When diffraction is neglected, the FEL wave equation can be written in the simplest form

$$\mathring{a} = -j\left\langle e^{-i\zeta}\right\rangle. \tag{III.39}$$

The dimensionless current density j measures the coupling between the electron beam and the optical mode, and $\left\langle e^{-i\zeta}\right\rangle$ measures the amount of electron bunching. When j is large ($j \gg \pi$), the coupling is large and we have high gain; when j is small($j \lesssim \pi$) we have low gain.

3. Gain

Until now, we have studied the interaction between free electrons in the beam and laser light through the Lorentz force equations in the helical undulator. Previ-

ously, we have understood the bunching of electrons in phase space resulting in coherent radiation through the pendulum equation. Now, we have coupled this bunching to the laser beam through the FEL wave equation.

When we assume a weak field $\mid a \mid \lesssim \pi$ and low gain $j \lesssim \pi$, we can apply a pertubation expansion to the pendulum equation, resulting in FEL gain, [2]

$$G(\tau) = \frac{\mid a(\tau) \mid^2}{{a_0}^2} - 1 = jF\left(\frac{2 - 2\cos(\nu_0\tau) - \nu_0\tau\sin(\nu_0\tau)}{{\nu_0}^3}\right), \qquad \text{(III.40)}$$

where a filling factor F represents a ratio of cross sectional areas of electron beam to optical mode such as $F = (r_b/w_0)^2$ at the waist of the mode, where r_b is the electron beam radius and w_0 is the optical mode waist radius. Gain is proportional to the dimensionless current density j and filling factor F, and the final gain spectrum at $\tau = 1$ depends only on the initial electron phase velocity ν_0 as shown in Figure 12. As seen before, there is no gain at resonance, $\nu_0 = 0$, and the peak of G/jF (gain normalized to j and F) is about 13.5% and occurs at $\nu_0 \approx 2.6$. //

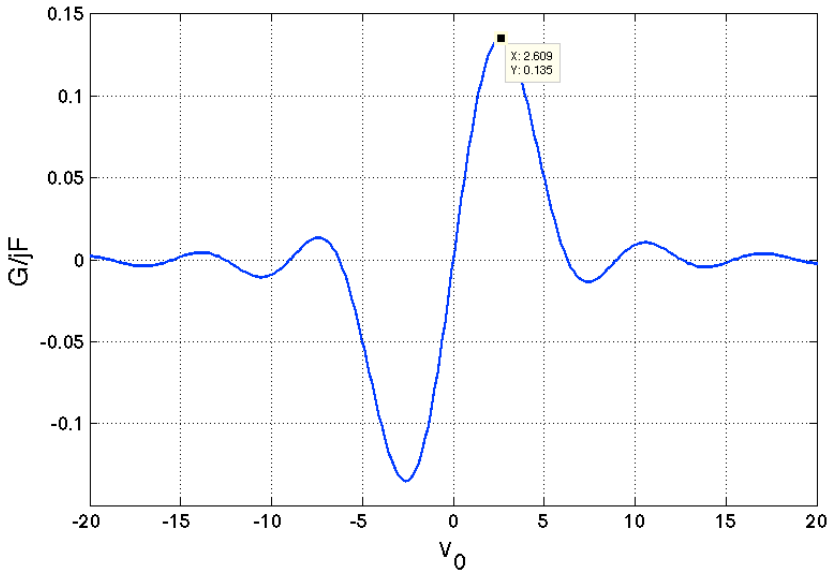

Figure 12. Single pass G/jF versus initial electron phase velocity ν_0 at $\tau = 1$.

4. Extraction

In order to describe the energy exchange between the electron beam and optical field, we estimate the extraction η defined as the fractional energy transferred from the electron beam to the optical field during a single pass through the undulator [6]:

$$\eta \equiv \frac{E_{opt}}{E_b} = \frac{\langle \Delta E \rangle}{E_b} = \frac{\langle \Delta \gamma \rangle}{\gamma}, \tag{III.41}$$

where E_{opt} and E_b are the energy in the optical field and the electron beam, respectively, in a common volume element of the beams, and $\Delta E = \Delta \gamma mc^2$ is the net change in the electron beam energy through the undulator. Applying Equation (III. 24) to (III. 41) allows us to have the following result:

$$\eta_{max} = \frac{\langle \Delta \gamma \rangle}{\gamma} = \frac{\langle \Delta \nu \rangle}{4\pi N} \approx \frac{1}{2N}, \tag{III.42}$$

where it has been assumed that approximately half the electrons lose energy across the positive gain bandwidth $\Delta\nu \sim \pi$ illustrated in Figure 12. We know the height of the separatrix is $4\sqrt{a}$, as presented below Equation (III. 27). This height corresponds to a change of an electron phase velocity $\Delta\nu$, when an electron is in the largest closed orbit. Suppose that only half of the electrons are in closed orbits, then $\langle \Delta\nu \rangle$ would be $2\sqrt{a}$. Now, we need to prove that $a \sim \pi^2$ by giving a short account of "Synchrotron" oscillation.

Another argument starts from phase space considerations. Start with the pendulum equation with low gain $j \lesssim \pi$ and strong fields $\mid a \mid \gtrsim \pi$. Assuming $\mid a \mid \approx$ constant and $\phi = 0$ yields the pendulum equation as

$$\overset{\circ\circ}{\zeta} = \mid a \mid \cos(\zeta). \tag{III.43}$$

For an electron trapped in strong field near the stable fixed point $(\zeta_0 = \pi/2, 0)$ in the phase space, its motion can be described by

$$\zeta(\tau) = \frac{\pi}{2} + x(\tau), \tag{III.44}$$

where $\zeta_0 = \pi/2$ is the initial electron position and $x(\tau) \ll \pi$ [2]. Substituting Equation (III. 44) into (III. 43) gives

$$\overset{\circ\circ}{x} = \mid a \mid \cos\left(\frac{\pi}{2} + x\right) \approx - \mid a \mid x = -{\nu_s}^2 x, \tag{III.45}$$

where ν_s is the synchrotron frequency about the stable fixed point $\zeta_0 = \pi/2$. We recognize that the simple harmonic oscillation of electrons around the stable fixed point $(\pi/2, 0)$ has the frequency $\nu_s = \mid a \mid^{1/2}$. The trapped electrons will execute approximately half a synchrotron oscillation at saturation, or $\nu_s \approx \pi$ when $\mid a \mid \approx \pi^2$. Assuming about half the electrons are trapped, we arrive at the estimate for extraction

$$\eta_{max} = \frac{\langle \Delta\gamma \rangle}{\gamma} = \frac{\langle \Delta\nu \rangle}{4\pi N} \approx \frac{2\sqrt{a}}{4\pi N} \approx \frac{1}{2N} \tag{III.46}$$

THIS PAGE INTENTIONALLY LEFT BLANK

IV. HERMITE GAUSSIAN RESONATOR MODES

In the previous chapter, we examined the interaction between the electron beam and the optical field inside the undulator. This chapter examines the wave nature of laser beams as they propagate in free space. Up to this point, we have assumed the optical beam to consist of plane waves neglecting diffraction. The wave usually takes the form of a Gaussian beam as defined by the optical cavity bounded by spherical resonator mirrors. In order to understand the characteristics of a Gaussian beam, we will find solutions to the free-space wave equation including diffraction.

A. SOLUTION OF WAVE EQUATION

The characteristics of Gaussian laser beams in a resonator have been analyzed by Siegman [12], Kogelnik [13], Pedrotti [14], and others. This chapter follows their analysis.

1. Scalar Wave Equation

Let us consider a general wave equation for the vector potential $\mathbf{A}$ without a current source,

$$\left(\nabla^2 - \frac{1}{c^2}\frac{\partial^2}{\partial t^2}\right)\mathbf{A} = 0 \quad \text{or} \quad \nabla^2\mathbf{A} = \frac{1}{c^2}\frac{\partial^2\mathbf{A}}{\partial t^2}. \tag{IV.1}$$

Assuming $A(x,y,z,t) = u(x,y,z)T(t)$ and utilizing a process of separation of variables, we have

$$\underbrace{\frac{1}{u}\nabla^2 u}_{\text{space}} = \underbrace{\frac{1}{c^2}\frac{1}{T}\frac{\mathrm{d}^2T}{\mathrm{d}t^2}}_{\text{time}} = \text{constant} = -k^2, \qquad k \geq 0, \tag{IV.2}$$

where the left-hand side is only a function of space and the right side is only a function of time, so that u represents a component of the electromagnetic field or of the vector potential $\mathbf{A}$. When we consider only the scalar function of space, u, we arrive at a scalar wave equation, the Helmholtz equation [15]

$$\left(\nabla^2 + k^2\right)u(x,y,z) = 0, \tag{IV.3}$$

where $k = 2\pi/\lambda$ is the propagation constant in the medium, with a harmonic time variation, $e^{-i\omega t}$.

2. Fundamental Mode

For an optical beam traveling along the z-direction, Equation (IV.3) becomes

$$u(x, y, z) = \psi(x, y, z)e^{ikz}, \tag{IV.4}$$

where ψ is a slowly varying complex valued function, and e^{ikz} describes a plane-wave in the z-direction. Generally, ψ represents the distinction between the actual laser beam and a plane wave, which we will examine in detail below. Substituting Equation (IV.4) into the scalar wave Equation (IV.3) yields, in cartesian coordinates, the reduced equation

$$\frac{\partial^2\psi}{\partial x^2} + \frac{\partial^2\psi}{\partial y^2} + \frac{\partial^2\psi}{\partial z^2} + 2ik\frac{\partial\psi}{\partial z} = 0. \tag{IV.5}$$

As z ranges over an optical wavelength the change in ψ will be small, also the variation of ψ with respect to z will be much smaller than with respect to x and y. This slowly varying dependence of ψ on z can be expressed mathematically by the paraxial approximation [12]:

$$\left|\frac{\partial^2\psi}{\partial z^2}\right| \ll \left|2k\frac{\partial\psi}{\partial z}\right|, \qquad \left|\frac{\partial^2\psi}{\partial x^2}\right|, \quad \text{and} \quad \left|\frac{\partial^2\psi}{\partial y^2}\right|. \tag{IV.6}$$

We can then discard the second derivative of ψ with respect to z in Equation (IV.5) and obtain the paraxial wave equation:

$$\frac{\partial^2\psi}{\partial x^2} + \frac{\partial^2\psi}{\partial y^2} + 2ik\frac{\partial\psi}{\partial z} = 0. \tag{IV.7}$$

A form of solution for Equation (IV.7) in the fundamental mode can be written as [13]

$$\psi(x, y, z) = \exp\left[i\left(P(z) + \frac{k}{2q(z)}r^2\right)\right], \tag{IV.8}$$

where $r^2 = x^2 + y^2$, $P(z)$ is a complex phase shift which is related to the propagation of the optical beam, and $q(z)$ is the complex curvature of the phase front which represents the spherical shape of the Gaussian beam. We need to find these unknown

functions, $P(z)$ and $q(z)$. In order to get each term of Equation (IV.7), we take derivatives of ψ with respect to each component. We then have the following sources

$$\frac{\partial^2\psi}{\partial x^2} = \left(\frac{ik}{q} - \frac{k^2}{q^2}x^2\right)\psi, \tag{IV.9}$$

$$\frac{\partial^2\psi}{\partial y^2} = \left(\frac{ik}{q} - \frac{k^2}{q^2}y^2\right)\psi, \tag{IV.10}$$

and

$$\frac{\partial\psi}{\partial z} = \left(i\frac{\partial P}{\partial z} - \frac{ik}{2q^2}r^2\frac{\partial q}{\partial z}\right)\psi. \tag{IV.11}$$

Inserting Equations (IV.9), (IV.10), and (IV.11) into (IV.7) and dividing through by ψ, we arrive at

$$\frac{k}{q^2}r^2\left(\frac{\partial q}{\partial z} - 1\right) = 2\left(\frac{\partial P}{\partial z} - \frac{i}{q}\right). \tag{IV.12}$$

In order for Equation (IV.12) to be valid for any r^2, the expressions inside both parentheses must be zero. Therefore, we obtain the relations

$$\frac{\partial q}{\partial z} = 1\ , \tag{IV.13}$$

and

$$\frac{\partial P}{\partial z} = \frac{i}{q}\ . \tag{IV.14}$$

At this point, we should introduce two important parameters of the Gaussian beam, $w(z)$ and $R(z)$, where $w(z)$ is the beam radius or spot size, and $R(z)$ is the radius of curvature of the wavefront as shown in Figure 13. These parameters are associated with the waist spot size, w_0, and the ratio z/z_0 by the formulas [12]

$$w(z)^2 = {w_0}^2\left(1 + \frac{z^2}{{z_0}^2}\right), \tag{IV.15}$$

which can be derived from Equation (IV.13) and

$$R(z) = z\left(1 + \frac{{z_0}^2}{z^2}\right), \tag{IV.16}$$

where $z_0 \equiv \pi {w_0}^2/\lambda$, the Rayleigh length, is the distance which the beam travels from the waist to where the beam area doubles.

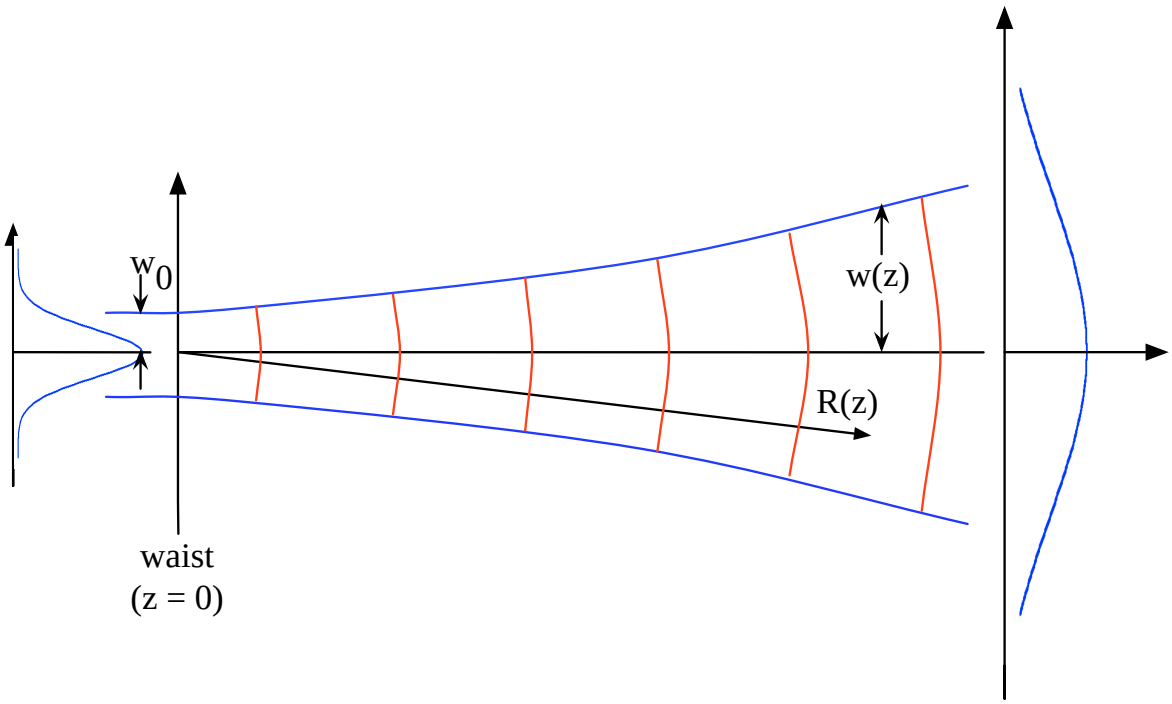

Figure 13. Notation for a fundamental Gaussian beam diverging away from its waist. w_0 is the waist spot size, $w(z)$ is the beam radius, and $R(z)$ is the radius of curvature. After [12]

We now consider Equation (IV.13); integrating this equation gives

$$q = z + q_0 = z - iz_0, \tag{IV.17}$$

where the initial value is $q_0 = -i\pi {w_0}^2/\lambda$ [13]. Starting with Equation (IV.17) and using Equations (IV.15) and (IV.16), we get the following result:

$$\frac{1}{q} = \frac{z}{z^2 + {z_0}^2} + i\frac{z_0}{z^2 + {z_0}^2} = \frac{1}{R} + i\frac{\lambda}{\pi w^2}. \tag{IV.18}$$

For convenience of later calculation, we can rewrite this equation as

$$\frac{k}{2q} = \frac{k}{2R} + \frac{ik\lambda}{2\pi w^2} = \frac{k}{2R} + \frac{i}{w^2}, \tag{IV.19}$$

where $k = 2\pi/\lambda$. To determine $P(z)$, we insert Equation (IV.17) into (IV.14) and we have

$$\frac{\partial P}{\partial z} = \frac{iz}{z^2 + {z_0}^2} - \frac{z_0}{z^2 + {z_0}^2}. \tag{IV.20}$$

Integration of this equation yields the following result

$$P(z) = i\left(\ln\sqrt{1+\frac{z^2}{{z_0}^2}}\right) - \tan^{-1}\frac{z}{z_0}. \tag{IV.21}$$

By using Equation (IV.15) we can rewrite this as

$$iP(z) = \ln\left(\frac{w_0}{w}\right) - i\tan^{-1}\frac{z}{z_0}, \tag{IV.22}$$

where the $\tan^{-1}(z/z_0)$ represents the phase shift difference between the Gaussian beam and a plane wave, and the amplitude factor, w_0/w, describes the decrease of the beam amplitude on the axis because of the expansion of the beam. Substituting Equations (IV.19) and (IV.22) into the trial solution, Equation (IV.8), we can finally obtain the solution of the fundamental mode:

$$\psi(x,y,z) = \frac{w_0}{w}e^{-r^2/w^2}\exp\left[i\left(\frac{kr^2}{2R} - \tan^{-1}\frac{z}{z_0}\right)\right]. \tag{IV.23}$$

Using this solution, Equation(IV.4) can be written in the form

$$u(r,z) = \underbrace{\frac{w_0}{w}e^{-r^2/w^2}}_{\text{Amplitude}}\exp\left[i\left(kz + \underbrace{\frac{kr^2}{2R} - \tan^{-1}\frac{z}{z_0}}_{\text{Phase }\phi}\right)\right]. \tag{IV.24}$$

Gaussian beams do not change their profile, but beams which have long wavelengths will be expanded significantly due to diffraction as they propagate. Figure 14 shows well the expansion of Gaussian beams. In order to show the expansion, we set the wavelength to $\lambda = 300\mu$m.

3. Higher Order Modes

In the previous section, we discussed only the lowest-order solution of Equation (IV.7). There are other higher-order solutions for the Equation (IV.7); these can take the form either of Hermite-Gaussian functions in cartesian coordinates or of Laguerre-Gaussian functions in cylindrical coordinates [12]. The properties of Laguerre-Gaussian modes in the FEL were analyzed by A. Kampouridis [4]. Throughout the rest of this thesis, we will use the cartesian coordinates for consistency.

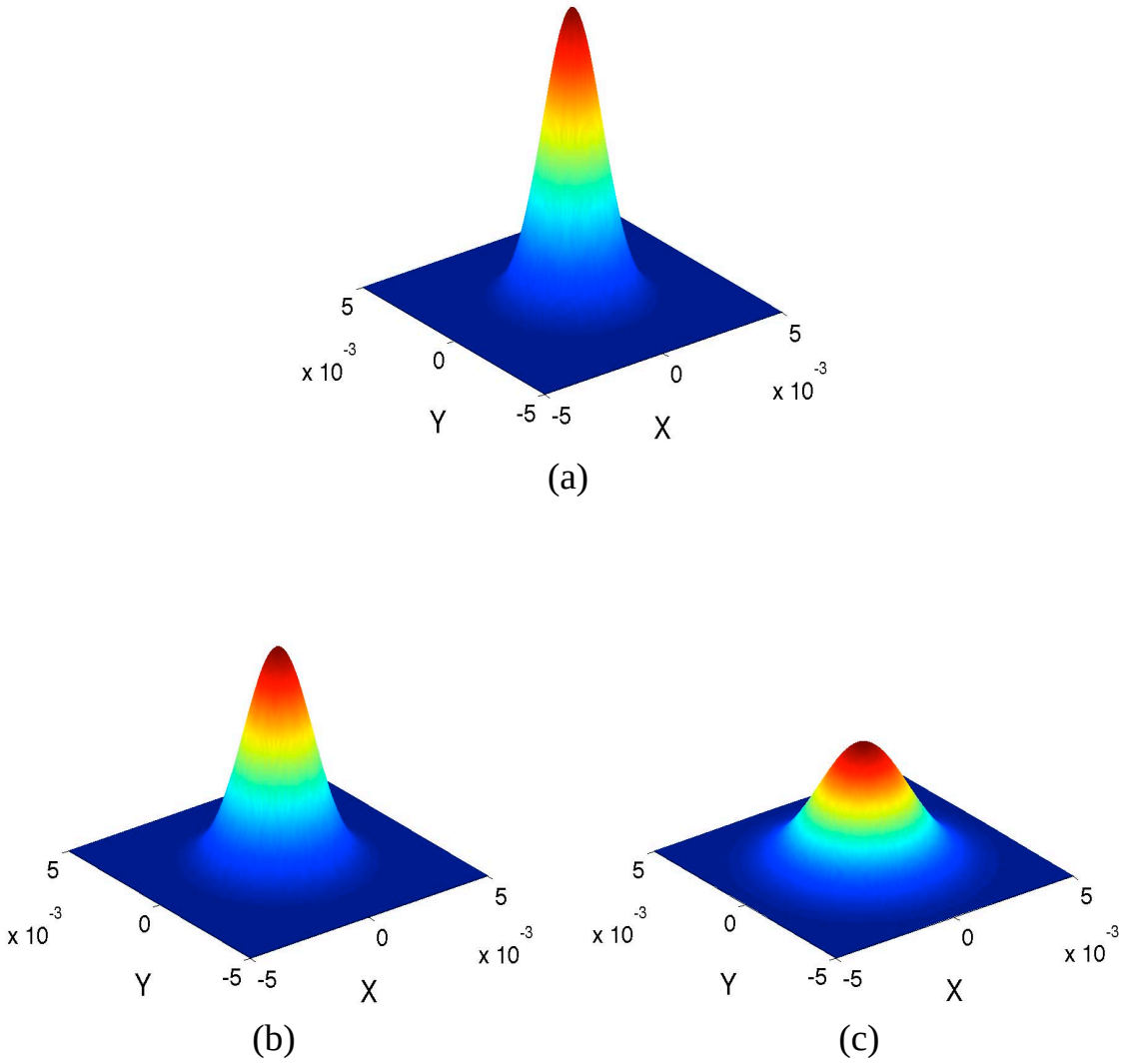

Figure 14. Surface plots of a Gaussian beam evolution as propagating along the z-axis. When we assume z=1m, (a) is an intensity profile at the beam waist (z=0.5m). At (b) (z=0.75m) and (c) (z=1m), we can see the expansion of the beam as it passes along the z-axis from the waist.

Let us assume a trial solution for Equation (IV.7) as

$$\psi = g\left(\frac{x}{w}\right) h\left(\frac{y}{w}\right) \exp\left[i\left(P(z) + \frac{k}{2q(z)} r^2\right)\right], \tag{IV.25}$$

where g is a function of x and z (because w depends on z), and h is a function of y and z to account for diffraction. Now, we should find $g(x/w)$, $h(y/w)$, $P(z)$, and $q(z)$ to get the complete solutions.

For convenience, let us find derivatives of g and h with respect to x and y. By using the chain rule, we get

$$\frac{\partial g}{\partial x} = \frac{\partial g}{\partial\left(x/w\right)} \frac{\partial\left(x/w\right)}{\partial x} = \frac{1}{w} \frac{\partial g}{\partial\left(x/w\right)} = \frac{1}{w} g',$$

$$\frac{\partial^2 g}{\partial x^2} = \frac{\partial}{\partial x}\left(\frac{\partial g}{\partial x}\right) = \frac{1}{w}\left(\frac{\partial g'}{\partial x}\right) = \frac{1}{w} \frac{\partial g'}{\partial\left(x/w\right)} \frac{\partial\left(x/w\right)}{\partial x} = \frac{1}{w^2} g'', \tag{IV.26}$$

and

$$\frac{\partial g}{\partial z} = \frac{\partial g}{\partial\left(x/w\right)} \frac{\partial\left(x/w\right)}{\partial z} = x \frac{\partial g}{\partial\left(x/w\right)}\left(-\frac{1}{w^2}\right) \frac{\partial w}{\partial z} = -\frac{x}{w^2} g' \frac{\partial w}{\partial z}, \tag{IV.27}$$

where $(..)' = \partial(..)/\partial\left(x/w\right)$. We can easily find the derivatives of h through similar processes:

$$\frac{\partial h}{\partial y} = \frac{1}{w} h' \ , \qquad \frac{\partial^2 h}{\partial y^2} = \frac{1}{w^2} h'' \tag{IV.28}$$

$$\frac{\partial h}{\partial z} = -\frac{y}{w^2} h' \frac{\partial w}{\partial z}. \tag{IV.29}$$

We are ready to take derivatives of Equation (IV.25). After some tedious work, we obtain the following results:

$$\frac{\partial^2 \psi}{\partial x^2} = e^{\left(iP + \frac{ik}{2q} r^2\right)}\left[\frac{1}{w^2} g'' h + \frac{2}{w} g' h\left(\frac{ik}{q} x\right) + gh\left(\frac{ik}{q}\right) - gh\left(\frac{k}{q} x\right)^2\right], \tag{IV.30}$$

$$\frac{\partial^2 \psi}{\partial y^2} = e^{\left(iP + \frac{ik}{2q} r^2\right)}\left[\frac{1}{w^2} g h'' + \frac{2}{w} g h'\left(\frac{ik}{q} y\right) + gh\left(\frac{ik}{q}\right) - gh\left(\frac{k}{q} y\right)^2\right], \tag{IV.31}$$

and

$$\frac{\partial \psi}{\partial z} = e^{\left(iP + \frac{ik}{2q} r^2\right)}\left(-\frac{1}{w^2} g' h \frac{\partial w}{\partial z} x - \frac{1}{w^2} g h' \frac{\partial w}{\partial z} y + ghi \frac{\partial P}{\partial z} - gh \frac{ikr^2}{2q^2} \frac{\partial q}{\partial z}\right). \tag{IV.32}$$

Substituting Equations (IV.30), (IV.31), and (IV.32) into (IV.7) and dividing by $gh\exp\left(iP+\frac{ik}{2q}r^2\right)$, we arrive at the following complicated equation

$$\underbrace{\frac{1}{w^2}\frac{g''}{g}+\frac{2ikx}{wq}\frac{g'}{g}-2ikx\frac{w_z}{w^2}\frac{g'}{g}}_{\text{independent of } y=-u_1}+\underbrace{\frac{1}{w^2}\frac{h''}{h}+\frac{2iky}{wq}\frac{h'}{h}-2iky\frac{w_z}{w^2}\frac{h'}{h}}_{\text{independent of } x=-u_2}$$

$$+\underbrace{r^2\left(-\frac{k^2}{q^2}+\frac{k^2}{q^2}\frac{\partial q}{\partial z}\right)}_{r^2 \text{ only}=0}+\underbrace{\frac{2ik}{q}-2k\frac{\partial P}{\partial z}}_{\text{no } r=u_1+u_2}=0. \tag{IV.33}$$

In order for this equation to have a solution, let us assume that the y-independent terms are $-u_1$ and the x-independent terms are $-u_2$. The r^2-dependent term should be identically zero since it must be valid for an any location in the transverse plane [11]. In the end, the terms left at the end should be u_1+u_2 so that the left-hand side sums to zero.

Let us consider the r^2 terms of Equation (IV.33) to get

$$r^2\frac{k^2}{q^2}\left(\frac{\partial q}{\partial z}-1\right)=0. \tag{IV.34}$$

We then have the familiar relation, $(\partial q/\partial z)=1$, which we have seen in the fundamental mode derivation. Thus, we have, easily:

$$\frac{1}{q}=\frac{1}{R}+i\frac{\lambda}{\pi w^2}. \tag{IV.35}$$

Next, multiplying the x-dependent terms of Equation (IV.33) by gw^2 and collecting terms in the derivatives of g, we have

$$g''+2ikx\left(\frac{w}{q}-\frac{\partial w}{\partial z}\right)g'+u_1w^2g=0. \tag{IV.36}$$

Let us calculate only the 2nd term. Recalling Equations (IV.15) and (IV.16) and substituting these two relations into the 2nd term, we have

$$2ikx\left(\frac{w}{R}+\frac{i\lambda}{\pi w}-\frac{\partial w}{\partial z}\right)g'=2ix\frac{2\pi}{\lambda}\left(\frac{i\lambda}{\pi w}\right)g'=-\frac{4x}{w}g',$$

where $\partial w/\partial z = w/R$. We can easily figure out this relation when we take the derivative of w with respect to z. We can then rewrite Equation (IV.36) as

$$g'' - \frac{4x}{w}g' + u_1 w^2 g = 0, \tag{IV.37}$$

which is close to a form of the Hermite equation $y'' - 2xy' + 2my = 0$ [16]. In order to transform Equation (IV.37) into the precise form of a Hermite equation, let

$$\chi = \sqrt{2}\frac{x}{w} \quad \rightarrow \quad \partial\left(\frac{x}{w}\right) = \frac{\partial\chi}{\sqrt{2}}. \tag{IV.38}$$

Then we have

$$g' = \frac{\partial g}{\partial\left(x/w\right)} = \sqrt{2}\frac{\partial g}{\partial\chi}\ , \quad g'' = 2\frac{\partial^2 g}{\partial\chi^2}. \tag{IV.39}$$

Inserting Equation (IV.39) into (IV.37) yields

$$\frac{\partial^2 g}{\partial\chi^2} - 2\chi\frac{\partial g}{\partial\chi} + 2mg = 0, \tag{IV.40}$$

which is exactly the same as the Hermite equation where $2m = u_1 w^2/2$. If $m = 0, 1, 2, \ldots$, then a solution of the Hermite equation is the Hermite polynomial $H_m(\chi)$ given by [16]

$$g(\chi) = H_m\left(\chi\right) = H_m\left(\sqrt{2}\frac{x}{w}\right) = (-1)^m e^{\chi^2}\frac{\mathrm{d}^m}{\mathrm{d}\chi^m}\left(e^{-\chi^2}\right). \tag{IV.41}$$

There are similar solutions for the y dependent terms of Equation (IV.33), i.e., $h(\xi) = H_n(\xi) = H_n\left(\sqrt{2}y/w\right)$, where $n = 0, 1, 2, \ldots$. Some of the Hermite polynomials of low-order are listed in Table I.

Now we are left with only the last terms of Equation (IV.33) which will give a solution for $P(z)$. According to Equation (IV.40), we know the fact that

$$u_1 = \frac{4m}{w^2}\ , \quad u_2 = \frac{4n}{w^2}.$$

By using these two relations, we rewrite the r-independent terms as

$$\frac{2ik}{q} - 2k\frac{\partial P}{\partial z} = u_1 + u_2 = \frac{4}{w^2}(m+n). \tag{IV.42}$$

$H_0(s) = 1$
$H_1(s) = 2s$
$H_2(s) = 4s^2 - 2$
$H_3(s) = 8s^3 - 12s$
$H_4(s) = 16s^4 - 48s^2 + 12$

Table 1. Hermite polynomials. From [16]

Substituting the middle terms of Equation (IV.18) into $1/q$, we obtain

$$\frac{\partial P}{\partial z} = \frac{i}{q} - \frac{2}{kw^2}(m+n) = \frac{iz}{z^2 + {z_0}^2} - (m+n+1)\frac{z_0}{z^2 + {z_0}^2}, \tag{IV.43}$$

where $2/(kw^2) = z_0/(z^2 + {z_0}^2)$. After integrating, we obtain

$$iP = \ln\left(\frac{w_0}{w}\right) - i(m+n+1)\tan^{-1}\frac{z}{z_0}, \tag{IV.44}$$

which is similar to Equation (IV.22) for the fundamental mode. Combining all sources, such as Equation (IV.41) for g, Equation (IV.44) for iP and Equation (IV.35) for $1/q$, we finally have the following solution for higher-order modes:

$$\psi_{m,n} = \frac{w_0}{w} H_m\left(\sqrt{2}\frac{x}{w}\right) H_n\left(\sqrt{2}\frac{y}{w}\right) e^{-r^2/w^2} \exp\left[i\left(\frac{kr^2}{2R} - (m+n+1)\tan^{-1}\frac{z}{z_0}\right)\right]. \tag{IV.45}$$

Utilizing this solution, Equation (IV.4) can be written in the form

$$u_{m,n} = \underbrace{\frac{w_0}{w} H_m\left(\sqrt{2}\frac{x}{w}\right) H_n\left(\sqrt{2}\frac{y}{w}\right) e^{-r^2/w^2}}_{\text{Amplitude}} \exp\left[i\left(kz + \underbrace{\frac{kr^2}{2R} - (m+n+1)\tan^{-1}\frac{z}{z_0}}_{\text{Phase } \phi}\right)\right], \tag{IV.46}$$

where the positive integers m and n identify the modes. These integer indices determine the shape of the beam intensity in the x and y direction, respectively. Several

examples of higher-order modes are shown in Figure 15. The intensity maxima are separated by anti-nodal lines. Note that mode label m equals the number of intensity anti-nodes proceeding from left to right, and n the number proceeding from top to bottom.

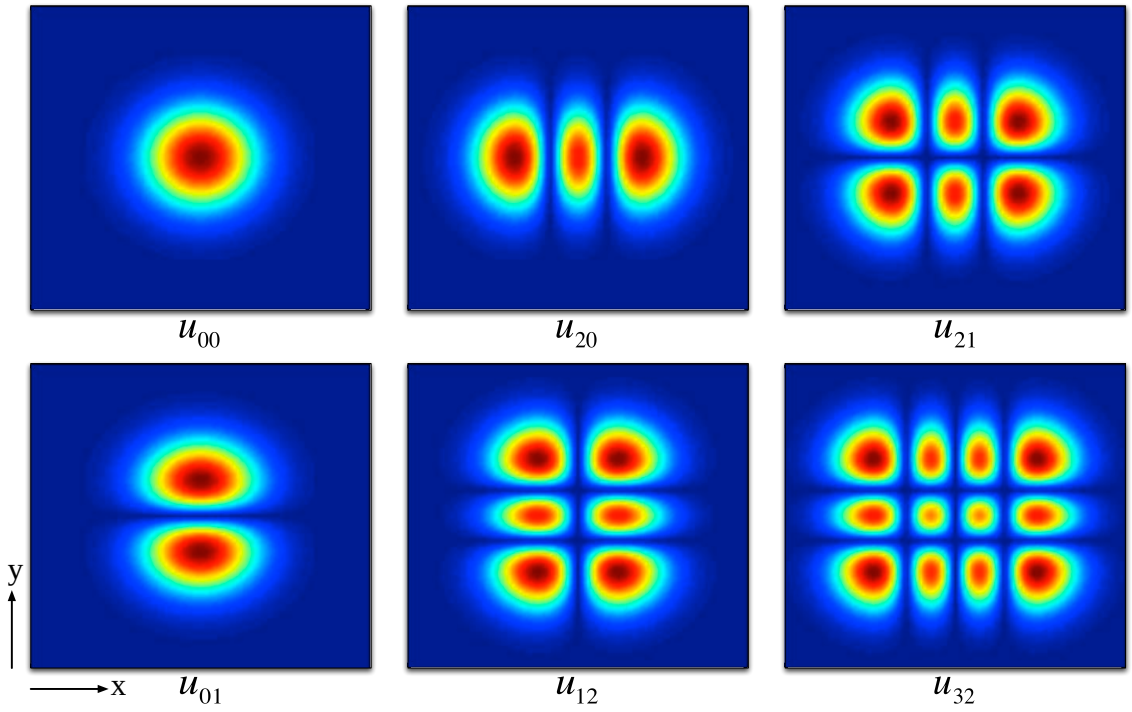

Figure 15. Intensity patterns for Hermite Gaussian modes in the transverse plane, x and y.

THIS PAGE INTENTIONALLY LEFT BLANK

V. FEL THEORY WITH HERMITE GAUSSIAN MODES

In the previous chapter, we found solutions of a wave equation for a Hermite Gaussian (HG) optical beam in free space. In the actual FEL operation, a beam of electrons interacts with the Gaussian optical beam, which is bounded by the spherical resonator mirrors, as shown in Figure 16.

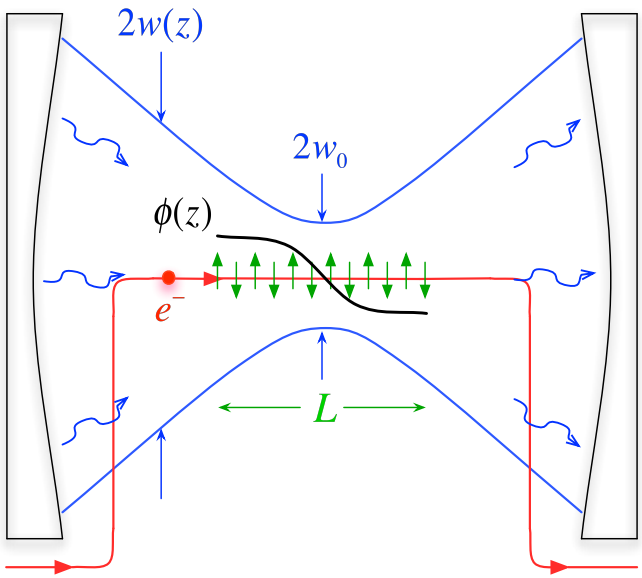

Figure 16. A schematic of the FEL oscillator shows the Gaussian beam (blue), with radius $w(z)$ expanding away from a waist w_0 centered in the undulator (green) of length L. Also, the optical phase $\phi(z)$ (black) changes along L. One electron path, on-axis at $r = 0$, is shown, and all transverse dimensions are exaggerated. After [24]

This chapter explores the FEL interaction, considering the characteristics of HG resonator modes. We will find a modified pendulum equation describing the microscopic electron evolution and determine the design of the HG mode which can maximize the interaction with the electron beam.

A. MODIFIED PENDULUM EQUATION

The electric field at the mode center ($r = 0$) in a fundamental Hermite Gaussian mode as derived in Chapter IV is

$$E(0,z) = E_0 \frac{w_0}{w(z)} \exp\left[i\left(kz + \phi(z)\right)\right], \tag{V.1}$$

where E_0 is the electric field amplitude at the mode waist, $k = 2\pi/\lambda$ is the mode wave number, and $\phi(z) = -\tan^{-1}\left[(z - L/2)/z_0\right]$ is the mode's phase. Also recall that the mode radius is $w(z) = w_0[1 + (z - L/2)^2/{z_0}^2]^{1/2}$, where $z_0 = \pi {w_0}^2/\lambda$ is the Rayleigh length, and w_0 is the mode waist radius at $z = L/2$. Although we will only deal with the fundamental Gaussian mode, results can easily be extended to higher-order modes [24]. The mode is centered at $\tau_w = 1/2$ ($z = L/2$), since this point is near a broad maximum in gain [24]. Using dimensionless time $\tau = z/L = ct/L$ in $w(z)$ and $\phi(z)$ gives

$$w^2(\tau) = {w_0}^2 \left[1 + \left(\frac{L}{z_0}\right)^2 \left(\tau - \frac{1}{2}\right)^2\right], \tag{V.2}$$

and

$$\phi(\tau) = -\tan^{-1}\left[\frac{L}{z_0}\left(\tau - \frac{1}{2}\right)\right]. \tag{V.3}$$

Recall the pendulum equation derived in the previous chapter:

$$\mathring{\zeta} = \mathring{\nu} = a(\tau)\cos\left[\zeta + \phi(\tau)\right], \tag{V.4}$$

where $a(\tau)$ is the dimensionless field amplitude in Equation (V.1) by $a(\tau) = a_0 w_0/w(\tau)$, where $a_0 = 4\pi NeKLE_0/\gamma^2 mc^2$ is the dimensionless optical wave amplitude. Inserting Equation (V.3) into (V.4) gives us the modified pendulum equation, describing an electron's evolution in an HG mode. The parameter L/z_0 compares the undulator length L with the Rayleigh length z_0. The Gaussian beam radius w and phase ϕ depend on L/z_0, as we saw in Equation (V.2) and (V.3). In order to illustrate some of the effects of the Gaussian beam, consider $L/z_0 \ll 1$ so that we almost have plane

waves [24]. To lowest order in L/z_0, we can then attain the following relations with $L/z_0 \ll 1$:

$$w(\tau) \approx w_0, \tag{V.5}$$

thus

$$a(\tau) = a_0 \frac{w_0}{w(\tau)} \approx a_0, \tag{V.6}$$

and

$$\phi(\tau) \approx -\frac{L}{z_0}\left(\tau - \frac{1}{2}\right), \tag{V.7}$$

using the small-angle approximation. Substituting Equations (V.6) and (V.7) into (V.4) yields the modified pendulum equation for the case of low gain ($j \lesssim \pi$)

$$\begin{aligned} \mathring{\zeta}=\mathring{\nu} &\approx a_0 \cos\left[\zeta_0 + \nu_0\tau - \frac{L}{z_0}\left(\tau - \frac{1}{2}\right)\right] \\ &\approx \underbrace{a_0}_{\text{field}} \cos\left[\underbrace{\zeta_0 + \frac{L}{2z_0}}_{\text{new phase}} + \tau \quad \underbrace{\left(\nu_0 - \frac{L}{z_0}\right)}_{\text{new resonance}}\right], \end{aligned} \tag{V.8}$$

where $\zeta = \zeta_0 + \nu_0\tau$, the solution of ζ to zeroth-order in a_0, has been used in weak optical fields ($a_0 \lesssim \pi$). The electrons have a new initial phase. But the shift $\zeta_0 \rightarrow \zeta_0 + L/2z_0$ in each phase is not significant since the beam is uniformly spread over each optical wavelength [24]. The gain spectrum has the form $\left[2 - 2\cos{\nu_0}^* - {\nu_0}^*(\sin{\nu_0}^*)\right]/{\nu_0}^{*3}$ derived in Chapter III, where now ${\nu_0}^* = \nu_0 - L/z_0$ in an HG mode. The gain spectrum is now shifted away from the exact resonance by an amount of L/z_0.

B. GAIN IN GAUSSIAN MODES

In a weak optical field $a_0 \lesssim \pi$ and for low gain $j \lesssim \pi$, the gain in the HG modes becomes

$$G(\tau) \propto jF_G, \tag{V.9}$$

where j is the dimensionless current density, and F_G is the filling factor for HG modes. Now, let us find the maximum filling factor averaged over the undulator length L in

order to get maximum gain. The averaged filling factor $\overline{F_G}$ is given by

$$\overline{F_G} = \frac{\text{electron beam area}}{\text{optical beam area}} = \frac{\pi {r_b}^2}{\pi \overline{w^2(z)}}, \tag{V.10}$$

where r_b is the electron beam radius (assumed constant), and $w(z)$ is the optical mode radius, $w^2(z) = {w_0}^2(1 + z^2/{z_0}^2)$. The area of the optical mode is given by

$$A(z) = \pi w^2(z) = \pi {w_0}^2 \left(1 + \frac{z^2}{{z_0}^2}\right). \tag{V.11}$$

The averaged area, therefore, becomes

$$\begin{aligned} \overline{A} &= \pi {w_0}^2 \frac{1}{L} \int_{-L/2}^{L/2} \left(1 + \frac{z^2}{{z_0}^2}\right) \, \mathrm{d}z \\ &= \pi {w_0}^2 \left(1 + \frac{L^2}{12{z_0}^2}\right) = \lambda \left(z_0 + \frac{L^2}{12 z_0}\right), \end{aligned} \tag{V.12}$$

where the Rayleigh length $z_0 = \pi {w_0}^2/\lambda$ has been used in the last step. In order to have maximum $\overline{F_G}$, we need to find the smallest value of $\overline{A}$ where $\mathrm{d}\overline{A}/\,\mathrm{d}z_0 = 0$:

$$\frac{\mathrm{d}\overline{A}}{\mathrm{d}z_0} = \lambda \left(1 - \frac{L^2}{12{z_0}^2}\right) = 0. \tag{V.13}$$

Consequently, the maximum filling factor, $\overline{F_G}^{\max}$, occurs at ${z_0}^{\max} = L/\sqrt{12} \approx (0.3)L$.

We have analytically derived that the gain spectrum is shifted by $\nu_0 \to \nu_0 - L/z_0$ when $L/z_0 \ll 1$. We have also shown analytically that the optimum gain occurs when $L/z_0 \sim 3$. Numerical simulations have shown that the shift in the gain spectrum still occurs for values of L/z_0 up to ~ 10, and is still roughly given by the approximate shift $\nu_0 \to \nu_0 - L/z_0$ [26].

VI. HYBRID (HG-WAVEGUIDE) RESONATOR MODES

For short wavelength operation of an FEL, an open resonator bounded by spherical reflecting mirrors is feasible, since the laser beam maintains a small cross-sectional area as it evolves along the interior of the undulator. However, when the FEL operates at long wavelengths, such as in the sub-millimeter or THz region, the expansion of the laser beam due to diffraction can be a problem, as shown in Figure 17.

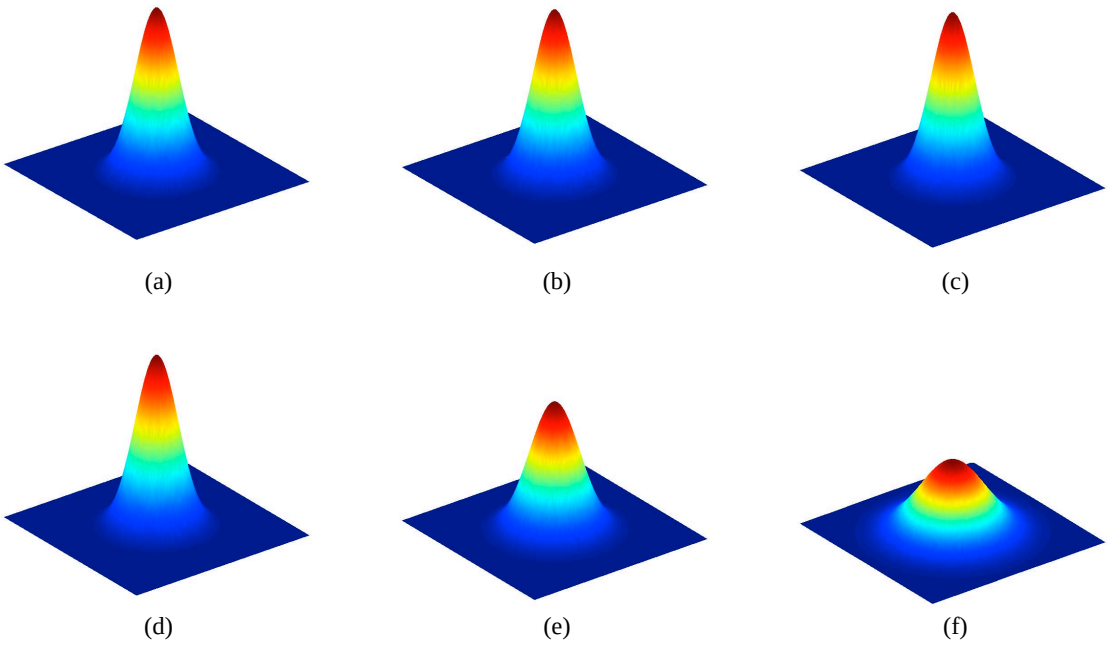

Figure 17. Surface plots of two Gaussian beams propagating along the z-axis without waveguides. Compared to the evolution of a short wavelength beam (Figures (a), (b) and (c) - 3μm), the evolution of a long wavelength beam (Figures (d), (e) and (f) - 30μm) obviously has a larger amount of expansion.

To accommodate lager diffraction at longer wavelengths, we need to have a larger undulator gap g, but the larger magnet spacing reduces the strength of the magnetic field according to $B = 1.95 B_{mag} \exp(-\pi g/\lambda_0)$, where λ_0 is the undulator period [2].

Consequently, the gain G will be decreased proportionally: $G \propto B^2$. A remedy is to use a waveguide structure, shown in Figure 18, to confine that the radiation. This chapter analyzes the Hermite Gaussian-Waveguide resonator modes, which will be designated as Hybrid resonator modes. The modes include characteristics of both Gaussian and waveguide modes. In order to understand the attributes of the waveguide, we solve the wave equation and explore the phase and group velocities of the laser pulse propagating through the waveguide.

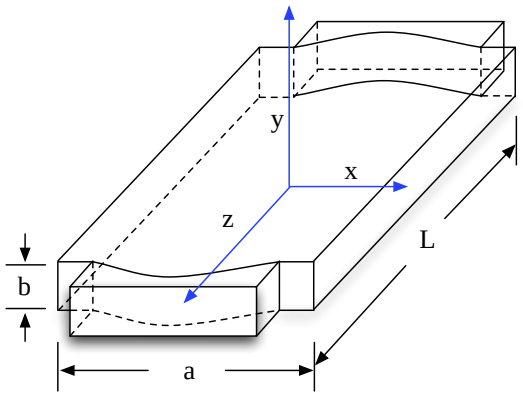

Figure 18. Geometry of a waveguide resonator. The origin is located at the center of the waveguide, with $y = 0$ at the bottom of the waveguide. Curved surfaces represent the mirrors. From [22]

A. SOLUTION OF WAVE EQUATION

The Hybrid resonator modes have been studied in detail by Elias [17], Degnan [18], and others. This section follows Elias's analysis, which is the basis of the UCSB FEL. To find solutions of a wave equation, assume that the electrical conductivity of the walls in Figure 18 are infinite. First find solutions to the wave equation inside a perfect, infinitely-long, rectangular waveguide in terms of Gaussian waves propagating along the z-axis. These manipulations are similar to the derivations of Chapter IV; the difference is that we need to consider waveguide properties in the y-direction.

1. Fundamental Mode

Each cartesian component of the electric (or magnetic) field must be satisfied by the Helmholz equation presented in Chapter IV:

$$\left(\nabla^2 + k^2\right) u(x, y, z) = 0, \tag{VI.1}$$

where $k = \omega/c = 2\pi/\lambda$, and a harmonic time variation, $e^{-i\omega t}$, has been assumed. Note that $u(x, y, z)$ can represent either a component of the electromagnetic field or of the vector potential of the light. We are interested in finding solutions describing Gaussian waves propagating along the z-axis without phase variations along the y-axis [17]. We express $u(x, y, z)$, an electromagnetic wave traveling along the z-direction within the waveguide, as

$$u(x, y, z) = \psi(x, z) e^{ik_n z} \sin\left(n\pi y/b\right), \tag{VI.2}$$

where $\psi(x, z)$ is a slowly-varying complex function, $e^{ik_n z}$ is a fast-varying carrier wave, $\sin(n\pi y/b)$, b is the distance between the top and bottom plates, and $n = \pm 1, \pm 2, \pm 3, \ldots$ is an integer in order to match boundary conditions at the walls of the waveguide (note $y = 0$ at the bottom wall). Inserting Equation (VI.2) into the scalar wave equation and dividing by $e^{ik_n z} \sin(n\pi y/b)$ yields

$$\frac{\partial^2 \psi}{\partial x^2} + \frac{\partial^2 \psi}{\partial z^2} + 2ik_n \frac{\partial \psi}{\partial z} + \psi \left[k^2 - \left(\frac{n\pi}{b}\right)^2 - {k_n}^2\right] = 0. \tag{VI.3}$$

From this equation, we find that

$$k_n = \sqrt{k^2 - \frac{n^2\pi^2}{b^2}}. \tag{VI.4}$$

When we apply the paraxial approximation [12], $\partial^2\psi/\partial z^2 \ll \partial^2\psi/\partial x^2$, and we arrive at the paraxial wave equation

$$\frac{\partial^2 \psi}{\partial x^2} + 2ik_n \frac{\partial \psi}{\partial z} = 0. \tag{VI.5}$$

Let us assume a trial solution of the form

$$\psi(x, z) = \exp\left[i\left(P(z) + \frac{k_n}{2q(z)} x^2\right)\right], \tag{VI.6}$$

similar to the Hermite-Gaussian case, except that here there is no y variable. We need to find the unknown functions $P(z)$ and $q(z)$ in a similar method to that described in Chapter IV. After inserting Equation (VI.6) into (VI.5) and comparing terms of equal power in x, we obtain the following relations

$$\frac{\partial q}{\partial z} = 1 \ , \tag{VI.7}$$

and

$$\frac{\partial P}{\partial z} = \frac{i}{2q} \ , \tag{VI.8}$$

In order to find $P(z)$ and $q(z)$, we use the definitions of $w(z)$ and $R(z)$ again, but these are not quite the same as the previous parameters since a new Rayleigh length, $z_R = {w_0}^2 k_n/2$ [17], differs from the previous one in Chapter IV, $z_0 = \pi {w_0}^2/\lambda = {w_0}^2 k/2$. Using this new definition of z_R, we integrate Equation (VI.7), yielding

$$q = z + q_0 = z - i\frac{{w_0}^2 k_n}{2} = z - iz_R, \tag{VI.9}$$

where the complex beam parameter at the waist is $q_0 = -i{w_0}^2 k_n/2$. Starting with Equation (VI.9), $q = z - iz_R$, and employing Equations (IV.15) and (IV.16) in Chapter IV, we obtain the following relation

$$\frac{k_n}{2q} = \frac{k_n}{2R} + \frac{i}{w^2}. \tag{VI.10}$$

To determine the $P(z)$, we insert Equation (VI.9) into (VI.8) and integrate the result, and we then have

$$iP(z) = \ln\left[\left(\frac{w}{w_0}\right)^{-\frac{1}{2}}\right] - \frac{i}{2}\tan^{-1}\frac{z}{z_R}, \tag{VI.11}$$

using the definition of $w(z)$. Substituting Equations (VI.10) and (VI.11) into the trial solution, Equation (VI.6), we can finally get the solution of the fundamental mode inside the waveguide

$$\psi(x,z) = \sqrt{\frac{w_0}{w}} e^{-x^2/w^2} \exp\left[i\left(\frac{k_n x^2}{2R} - \frac{1}{2}\tan^{-1}\frac{z}{z_R}\right)\right]. \tag{VI.12}$$

This solution for the fundamental mode is also similar to the Equation (IV.24) in Chapter IV, but now k_n appears instead of k, and the Gaussian form is only in the x-direction. Using this solution, Equation (VI.2) can be written in the form

$$u(x,y,z) = \underbrace{\sqrt{\frac{w_0}{w}}e^{-x^2/w^2}}_{\text{Amplitude}} \exp\left[i\left(\underbrace{k_n z + \frac{k_n x^2}{2R} - \frac{1}{2}\tan^{-1}\frac{z}{z_R}}_{\text{Phase }\phi}\right)\right] \sin\left(\frac{n\pi}{b}y\right). \quad \text{(VI.13)}$$

2. Higher-Order Modes

The higher-order solutions in the waveguide also take the form of Hermite-Gaussian functions in Cartesian coordinates, as we now show. Assume a trial solution to Equation (VI.5) in the form

$$\psi = g\exp\left[i\left(P + \frac{k_n}{2q}x^2\right)\right], \quad \text{(VI.14)}$$

where g is a function of x/w. We can easily find the derivatives of the unknown function g when we follow the notation mentioned in Chapter IV. They are

$$\frac{\partial^2\psi}{\partial x^2} = e^{\left(iP+\frac{ik_n}{2q}x^2\right)}\left[\frac{1}{w^2}g'' + \frac{2}{w}\left(\frac{ik_n}{q}x\right)g' + \left(\frac{ik_n}{q}\right)g - \left(\frac{k_n}{q}x\right)^2 g\right], \quad \text{(VI.15)}$$

and

$$\frac{\partial\psi}{\partial z} = e^{\left(iP+\frac{ik_n}{2q}x^2\right)}\left(-\frac{1}{w^2}g'\frac{\partial w}{\partial z}x + gi\frac{\partial P}{\partial z} - g\frac{ik_n x^2}{2q^2}\frac{\partial q}{\partial z}\right), \quad \text{(VI.16)}$$

where $(..)' = \partial(..)/\partial(x/w)$. Inserting Equations (VI.15) and (VI.16) into (VI.5) and dividing by $g\exp\left(iP + ik_n x^2/2q\right)$, we arrive at the following result

$$\underbrace{\frac{1}{w^2}\frac{g''}{g} + \frac{2ik_n x}{wq}\frac{g'}{g} - 2ik_n x\frac{\partial w/\partial z}{w^2}\frac{g'}{g}}_{x\text{ only} = u_1} + \underbrace{x^2\left(-\frac{{k_n}^2}{q^2} + \frac{{k_n}^2}{q^2}\frac{\partial q}{\partial z}\right)}_{x^2\text{ only} = 0} + \underbrace{\frac{ik_n}{q} - 2k_n\frac{\partial P}{\partial z}}_{\text{no } x = u_1} = 0. \quad \text{(VI.17)}$$

Utilizing the same notation as in Chapter IV allows us to have $g(x/w)$, $P(z)$, and $q(z)$ such that

$$g\left(\frac{x}{w}\right) = H_m\left(\frac{x}{w}\right), \qquad m = 0, 1, 2, \ldots, \quad \text{(VI.18)}$$

$$iP = \ln\left[\left(\frac{w}{w_0}\right)^{-\frac{1}{2}}\right] - i\left(m+\frac{1}{2}\right)\tan^{-1}\frac{z}{z_0}, \tag{VI.19}$$

and

$$\frac{1}{q} = \frac{1}{R} + \frac{2i}{k_n w^2}\ . \tag{VI.20}$$

Substituting these three equations into Equation (VI.14), we finally have the following solution for higher-order modes

$$\psi_{m,n} = \sqrt{\frac{w_0}{w}} H_m\left(\frac{x}{w}\right) e^{-x^2/w^2} \exp\left[i\left(\frac{k_n x^2}{2R} - \left(m+\frac{1}{2}\right)\tan^{-1}\frac{z}{z_R}\right)\right]. \tag{VI.21}$$

Utilizing this solution, we can express the optical beam, Equation (VI.2), as

$$u_{m,n} = \underbrace{\sqrt{\frac{w_0}{w}} H_m\left(\frac{x}{w}\right) e^{-x^2/w^2}}_{\text{Amplitude}} \exp\left[i\left(k_n z + \underbrace{\frac{k_n x^2}{2R} - \left(m+\frac{1}{2}\right)\tan^{-1}\frac{z}{z_R}}_{\text{Phase } \phi}\right)\right] \sin\left(\frac{n\pi}{b}y\right). \tag{VI.22}$$

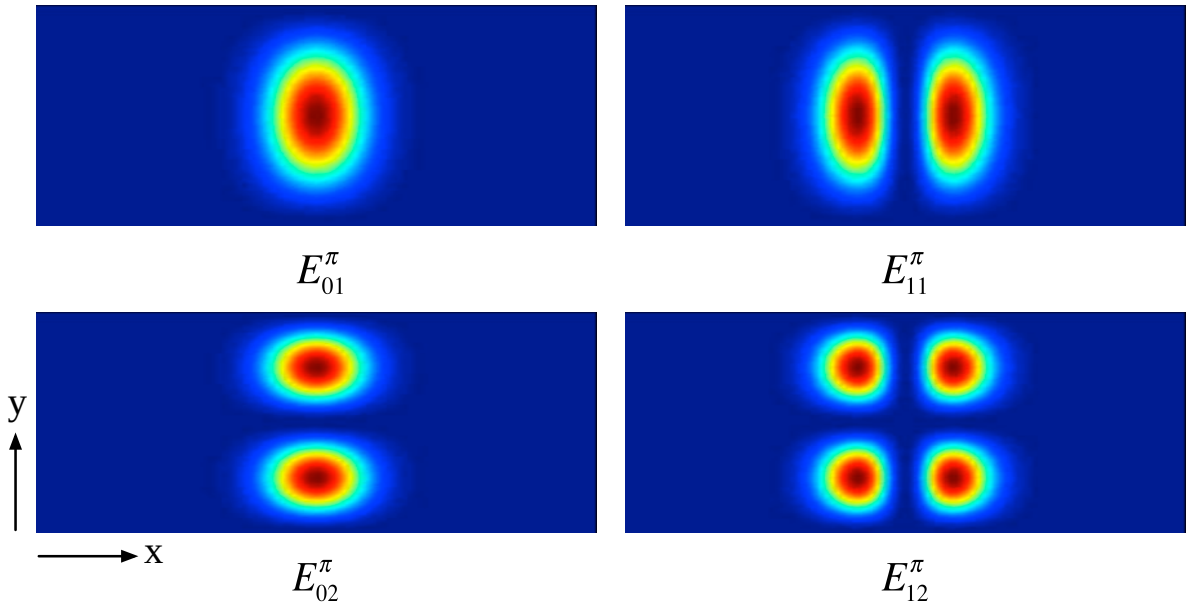

Figure 19. Intensity patterns $E^{\pi}{}_{mn}$ for Hybrid modes in the transverse plane, x and y.

Note that n, the waveguide constant in the sine function, differs from the previous n of H_n in Chapter IV. However, this n together with m determines the shape of the mode, as shown in Figure 19. We chose the $\sin(n\pi y/b)$ as a waveguide term in Equation (VI.2) to satisfy the boundary conditions; there are no fields for $n = 0$.

3. Solutions for ${E^{\pi}}_{mn}$ Modes

Elias and Gallardo [17] proposed two sets of linearly independent solutions differing by the choice of $\sin(n\pi y/b)$ or $\cos(n\pi y/b)$. In the solutions for $\sin(n\pi y/b)$, which will be designated as ${E^{\pi}}_{mn}$ modes, the dominant electric fields are parallel to the wide dimension of the waveguide, as shown in Figure 20.

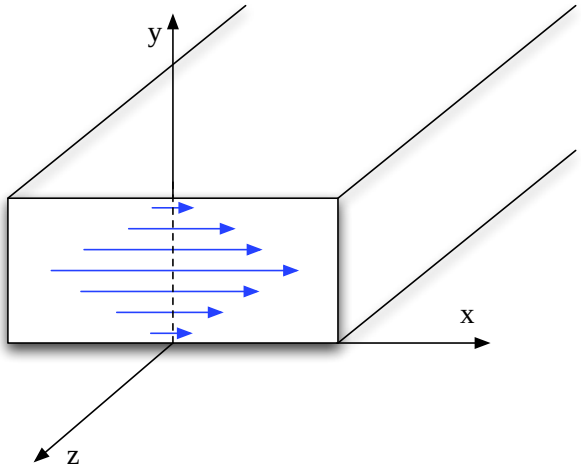

Figure 20. Electric field lines at the waist of the waveguide, which shows the ${E^{\pi}}_{01}$ mode.

The solutions for the choice $\cos(n\pi y/b)$, which will be designated as ${E^{\sigma}}_{mn}$ modes, the dominant electric fields are those which are perpendicular to the x-direction of the waveguide not shown in Figure 20. When we chose the ${E^{\pi}}_{mn}$ modes, waveguide losses are negligible since the electric fields near the plates are close to zero. In an FEL, the undulator magnets would be placed along the y-axis, so that an electron wiggles along the x-axis and couples to the electric fields of the mode, as shown in Figure 21.

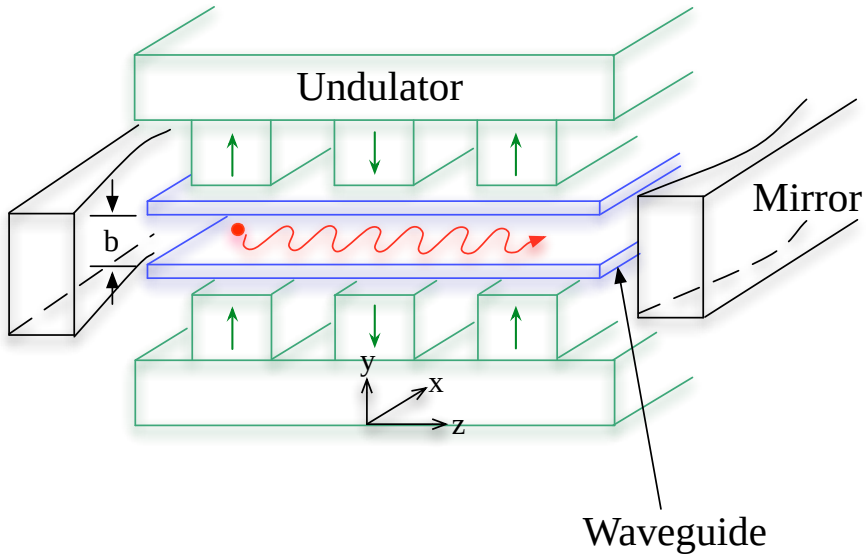

Figure 21. Schematic of a Hybrid resonator, showing the location of the critical components after [19]. The hybrid waveguide consists of a set of two parallel conducting plates separated by a distance b. A relativistic electron wiggles along the x-axis. A hole may be placed in the middle of the right mirror to allow output of the laser beam (KAERI is using this type of mirror for their FIR FEL [20]). Otherwise, a partially transparent mirror will be used for the out-coupling. In case of entry and exit of the electron beam, a chicane is usually used to bend the electron beam around the mirrors.

We are now ready to explore the solutions for ${E^{\pi}}_{mn}$ modes. Recall the proposed solution $u(x, y, z) = \psi(x, z)\sin(n\pi y/b)e^{ik_n z}$. We can then express the dominant electric fields E_x as

$$E_x \approx A_0 \psi_{mn} \sin\left(\frac{n\pi}{b} y\right) e^{ik_n z}, \tag{VI.23}$$

where A_0 is a constant. Using this equation and Maxwell's equation $\nabla \cdot \mathbf{E} = 0$ in free space, we can obtain the E_z component:

$$E_z \approx -\frac{A_0}{ik_n} \frac{\partial \psi_{mn}}{\partial x} \sin\left(\frac{n\pi}{b} y\right) e^{ik_n z}. \tag{VI.24}$$

Note that the E_x component is much greater than E_y and E_z, i.e., $E_x \gg E_y, E_z$. Also, $E_y = 0$, as represented by Figure 20. In order to determine the magnetic fields, we use Maxwell's equation $\nabla \times \mathbf{E} = -\partial \mathbf{B}/c\partial t$. When we consider only the y component

of this equation, we have

$$\frac{\partial B_y}{c\partial t} = -\frac{\partial E_x}{\partial z} \approx -(ik_n)A_0\psi_{mn}\sin\left(\frac{n\pi}{b}y\right)e^{ik_n z},$$

and

$$B_y \approx \frac{k_n c}{\omega}A_0\psi_{mn}\sin\left(\frac{n\pi}{b}y\right)e^{ik_n z}, \tag{VI.25}$$

where $\partial\psi_{mn}/\partial z$ has been ignored, since the amplitude of the longitudinal components of the fields are much smaller than the corresponding transverse components, and the harmonic variation $e^{-i\omega t}$ has been assumed, respectively. Next, let us discuss the z component of $\nabla \times \mathbf{E} = -\partial\mathbf{B}/c\partial t$. We then have

$$\frac{\partial B_z}{c\partial t} = \frac{\partial E_x}{\partial y} \approx \frac{n\pi}{b}A_0\psi_{mn}\cos\left(\frac{n\pi}{b}y\right)e^{ik_n z},$$

and

$$B_z \approx -\frac{n\pi c}{bi\omega}A_0\psi_{mn}\cos\left(\frac{n\pi}{b}y\right)e^{ik_n z}, \tag{VI.26}$$

where a harmonic variation $e^{-i\omega t}$ has been assumed again. Lastly, the boundary conditions applied on the ${E^\pi}_{mn}$ modes are $E_x, E_z = 0$ at $y = 0$ and $y = b$. A summary of the ${E^\pi}_{mn}$ modes solutions is given by the following table.

$E_x \approx A_0\psi_{mn}\sin(n\pi y/b)e^{ik_n z}$
$E_y = 0$
$E_z \approx -\left(A_0/ik_n\right)\left(\partial\psi_{mn}/\partial x\right)\sin(n\pi y/b)e^{ik_n z}$

Table 2. ${E^\pi}_{mn}$ - modes solutions

Starting with these solutions, we find a relation between the coefficient A_0 and the power of the electromagnetic field. The expression for total energy density [21] is:

$$u = \frac{1}{2}(E^2 + B^2). \tag{VI.27}$$

Multiplying the speed of light c by the energy density yields the power per unit area:

$$\frac{\text{Power}}{\text{Area}} = \frac{c}{2}(E^2 + B^2). \tag{VI.28}$$

We can then find the power by integrating Equation (VI.28), yielding

$$P = \int \left(\frac{\text{Power}}{\text{Area}}\right) \, \mathrm{d}x \, \mathrm{d}y = \frac{c}{2}\int (E^2 + B^2) \, \mathrm{d}x \, \mathrm{d}y. \tag{VI.29}$$

Inserting the dominant electric and magnetic fields from the solutions gives

$$\begin{aligned} P &= c{A_0}^2 \int_{-\infty}^{\infty} e^{-2x^2/{w_0}^2} \, \mathrm{d}x \int_0^b \sin^2\left(\frac{\pi}{b}y\right) \, \mathrm{d}y \\ &= c{A_0}^2 w_0 \frac{b\sqrt{\pi}}{2\sqrt{2}}, \end{aligned} \tag{VI.30}$$

where we have used the fundamental mode $n = 1$, assumed $k_1 \approx k$, and $w(z) = w_0$ (at the waist) for convenience in calculation. Finally, we have the coefficient A_0:

$$A_0 = \sqrt{\frac{2\sqrt{2}P}{b\sqrt{\pi}cw_0}}. \tag{VI.31}$$

B. PHASE AND GROUP VELOCITY

The general expressions for phase and group velocities of a electromagnetic wave are $v_p \equiv \omega/k$, and $v_g \equiv \ \mathrm{d}\omega/\ \mathrm{d}k$.Then from Equation (VI.4) with $z \ll z_R$, we have:

$$\frac{{k_n}^2}{\omega^2} = \frac{1}{{v_{pn}}^2} = \frac{1}{c^2} - \left(\frac{n\pi}{\omega b}\right)^2.$$

Therefore,

$$v_{pn} = \frac{c}{\sqrt{1 - (n\pi c/\omega b)^2}}. \tag{VI.32}$$

Note that the phase velocity of the wave depends on the waveguide number, $n = 1, 2, 3, \ldots$, the frequency, ω, and the height of the waveguide, b. Also, the phase velocity, v_{pn}, is faster than the speed of light, c, since

$$v_{pn} = \frac{\omega}{k_n} = \frac{c}{\sqrt{1 - (n\pi c/\omega b)^2}} \quad > \quad c.$$

The group velocity of the wave can be derived from Equation (VI.4). Differentiating this equation with respect to ω, we get

$$2k_n \frac{\mathrm{d}k_n}{\mathrm{d}\omega} = 2\frac{\omega}{c^2} \quad \rightarrow \quad \frac{\mathrm{d}k_n}{\mathrm{d}\omega} = \frac{\omega}{k_n c^2}. \tag{VI.33}$$

Hence, the group velocity is

$$v_{gn} = \frac{\mathrm{d}\omega}{\mathrm{d}k_n} = \frac{k_n^2 c}{\omega} = \frac{c^2}{v_{pn}}. \tag{VI.34}$$

We can rewrite Equations (VI.43) and (VI.45) as

$$v_{pn} = \frac{c}{\sqrt{1-(n\pi c/\omega b)^2}} = \frac{c}{\sqrt{1-(cn\cancel{\pi}/2\cancel{\pi}fb)^2}} = \frac{c}{\sqrt{1-(n\lambda/2b)^2}}, \tag{VI.35}$$

and

$$v_{gn} = \frac{c^2}{v_{pn}} = c\sqrt{1-\left(\frac{n\lambda}{2b}\right)^2}. \tag{VI.36}$$

Thus, $v_{pn}v_{gn} = c^2$ is also satisfied inside the waveguide.

Note that when the wavelength is equal to the cut-off wavelength, i.e., $\lambda_c = 2b$ and $\theta = 90°$ as shown in Figure 22, the phase velocity is infinite and the group velocity is zero so that no energy propagates along the waveguide.

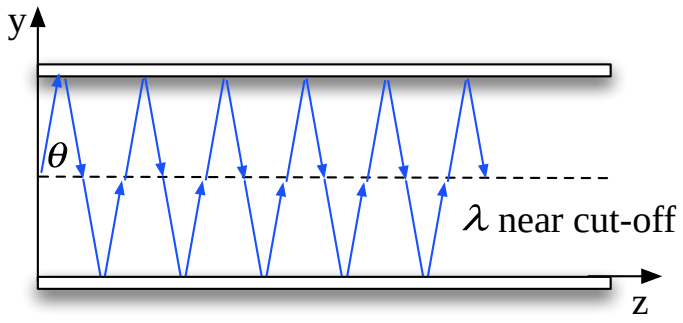

Figure 22. A sinusoidal electromagnetic wave entering one end of the waveguide with its electric field parallel to the wide dimension and propagating at an angle θ will be successively reflected by the top and bottom walls and follow a zig-zag path. λ is near the cut-off wavelength. From [23]

The cut-off frequency f_c is given by

$$f_c = \frac{c}{\lambda_c} = \frac{c}{2b}. \tag{VI.37}$$

Using this equation, we can rewrite the phase and group velocity in terms of frequency as

$$v_{pn} = \frac{c}{\sqrt{1-(n\lambda/2b)^2}} = \frac{c}{\sqrt{1-(n\lambda/\lambda_c)^2}} = \frac{c}{\sqrt{1-(nf_c/f)^2}}, \tag{VI.38}$$

and

$$v_{gn} = c\sqrt{1-\left(\frac{n\lambda}{2b}\right)^2} = c\sqrt{1-\left(\frac{n\lambda}{\lambda_c}\right)^2} = c\sqrt{1-\left(\frac{nf_c}{f}\right)^2}. \tag{VI.39}$$

VII. FEL THEORY WITH HYBRID (HG-WAVEGUIDE) MODES

A Hybrid mode occurs in a waveguide consisting of two flat conducting plates seperated by a distance b, each parallel to the x-z plane. This waveguide serves as an optical beam pipe between the resonator mirrors. In principle, there are image charges in the conducting walls that may affect the electron trajectories, but they are very small. More important things are the space charge forces in the beam itself which are assumed negligible here, as in most FELs. In this chapter, we will explore a modified pendulum equation appropriate to Hybrid modes. We will then design the relevant FEL which results in maximum energy gain, using the same analysis as in Chapter V.

A. MODIFIED PENDULUM EQUATION

The electric field at the mode center ($x = 0$, $y = b/2$) in a fundamental Hybrid mode as derived in Chapter VI is

$$E\left(0, \frac{b}{2}, z\right) = E_0 \sqrt{\frac{w_0}{w(z)}} \exp\left[i\left(k_1 z + \phi(z)\right)\right], \tag{VII.1}$$

where E_0 is the electric field amplitude at the mode waist, $k_1 = \sqrt{k^2 - \pi^2/b^2}$, and $\phi(z) = -0.5 \tan^{-1}\left[(z - L/2)/z_R\right]$, where $z_R = {w_0}^2 k_1/2$ is the Rayleigh length for this Hybrid mode case, and w_0 is the mode waist radius at $z = L/2$. Although we will only deal with the fundamental Hybrid mode, results can easily be extended to higher-order modes. We can again introduce the dimensionless time, $\tau = z/L$, so that the mode is centered at $\tau_w = 1/2$, near a broad maximum in gain [24]. Through a derivation similar to that in Chapter V, we have

$$w^2(\tau) = {w_0}^2 \left[1 + \left(\frac{L}{z_R}\right)^2 \left(\tau - \frac{1}{2}\right)^2\right], \tag{VII.2}$$

and

$$\phi(\tau) = -\frac{1}{2} \tan^{-1}\left[\frac{L}{z_R}\left(\tau - \frac{1}{2}\right)\right]. \tag{VII.3}$$

Our original pendulum equation in Chapter III is

$$\mathring{\zeta} = \mathring{\nu} = a(\tau)\cos\left[\zeta + \phi(\tau)\right], \tag{VII.4}$$

where $a(\tau)$ is the amplitude factor in Equation (VII.1), where $a_0 = 4\pi NeKLE_0/\gamma^2 mc^2$ is the dimensionless optical wave amplitude. Using the approximation, $L/z_R \ll 1$ describing a near plane wave, gives us to lowest order in L/z_R

$$w(\tau) \approx w_0, \tag{VII.5}$$

so that

$$a(\tau) = a_0\sqrt{\frac{w_0}{w(\tau)}} \approx a_0, \tag{VII.6}$$

and

$$\phi(\tau) \approx -\frac{L}{2z_R}\left(\tau - \frac{1}{2}\right). \tag{VII.7}$$

Substituting Equation (VII.6) and (VII.7) into (VII.4) yields the modified pendulum equation for the case of low gain ($j \lesssim \pi$), derived here for the first time:

$$\begin{aligned}\mathring{\zeta} = \mathring{\nu} &\approx a_0\cos\left[\zeta_0 + \nu_0\tau - \frac{L}{4z_R}\left(\tau - \frac{1}{2}\right)\right] \\ &\approx \underbrace{a_0}_{\text{field}}\cos\left[\underbrace{\zeta_0 + \frac{L}{4z_R}}_{\text{new phase}} + \tau\ \underbrace{\left(\nu_0 - \frac{L}{2z_R}\right)}_{\text{new resonance}}\right],\end{aligned} \tag{VII.8}$$

where $\zeta = \zeta_0 + \nu_0\tau$ has been used assuming weak optical fields ($a_0 \lesssim \pi$). The electron has a new initial phase $\zeta_0 + L/2z_R$, but this shift can be ignored because the electrons are uniformly spread along each optical wavelength. However, we cannot ignore the new resonance parameter, $\nu_0 \rightarrow (\nu_0 - L/2z_R)$, which causes a measurable change in the FEL operation. In a weak optical field $a_0 \lesssim \pi$, the gain spectrum has the form $\left[2 - 2\cos\nu_0{}^* - \nu_0{}^*(\sin\nu_0{}^*)\right]/\nu_0{}^{*3}$ derived in Chapter III, where now $\nu_0{}^* = \nu_0 - L/2z_R$ in the Hybrid mode.

B. GAIN IN HYBRID MODES

In a fundamental Hybrid mode, the transverse mode area can be used to calculate the filling factor. This affects the gain, since gain is proportional to the filling factor ($G \propto jF_H$). The cross-section area of the elliptical Hybrid mode can be expressed $\pi r_x r_y$, where $r_x = w(z)$, $r_y \approx b/2$, and b is the height of the waveguide as shown in Figure 23.

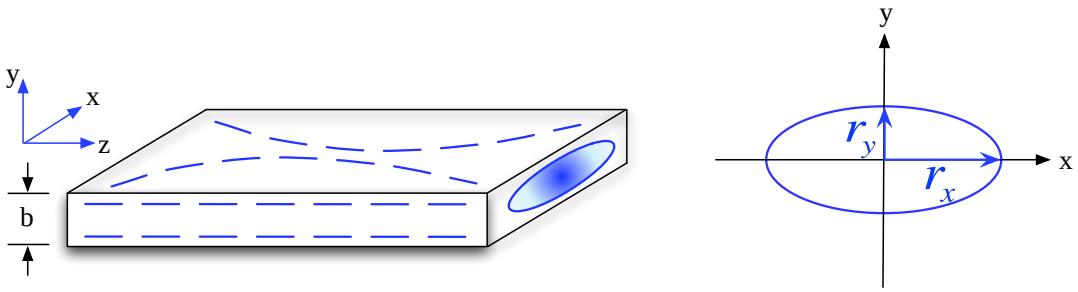

Figure 23. Cross-section of the fundamental Hybrid mode. The area of the elliptical cross section of the mode is $\pi r_x r_y \approx \pi w(z) b/2$.

By using a similar analysis as in Chapter V, we can find what z_R value gives the maximum $\overline{F_H}$, which leads to the maximum gain. In a weak optical field $a_0 \lesssim \pi$, the gain for the fundamental Hybrid mode is given by

$$G(\tau) \propto jF_H, \tag{VII.9}$$

where j is the dimensionless current density, and F_H is the new filling factor for the Hybrid mode, which we will explore in detail through this section. The averaged filling factor $\overline{F_H}$ becomes

$$\overline{F_H} = \frac{\text{electron beam area}}{\text{optical beam Area}} = \frac{2\pi {r_b}^2}{\pi b \overline{w(z)}}, \tag{VII.10}$$

where r_b is the electron beam radius (assumed constant), $w(z)$ is the optical mode semi-major axis along x, and $b/2$ is the optical mode semi-minor axis along y. We can write the area of the fundamental Hybrid mode as

$$A(z) = \frac{\pi b}{2} w(z) = \frac{\pi b}{2} w_0 \left(1 + \frac{z^2}{{z_R}^2}\right)^{1/2}, \tag{VII.11}$$

where $z_R = {w_0}^2 k_1/2$, and $k_1 = (k^2 - \pi^2/b^2)^{1/2}$. Thus, the averaged mode area becomes

$$\begin{aligned}\overline{A} &= \frac{1}{L}\int_{-L/2}^{L/2} A(z)\,\mathrm{d}z = \frac{\pi b w_0}{2L}\int_{-L/2}^{L/2}\left(1+\frac{z^2}{{z_R}^2}\right)^{1/2} \\ &= \frac{\pi b w_0 z_R}{2L}\left[\frac{L}{2z_R}\left(\frac{L^2}{4{z_R}^2}+1\right)^{1/2} + \ln\left\{\frac{L}{2z_R}+\left(\frac{L^2}{4{z_R}^2}+1\right)^{1/2}\right\}\right] \\ &= \frac{\pi b}{\sqrt{2k_1}L}\left[\frac{\sqrt{z_R}L}{2}\left(\frac{L^2}{4{z_R}^2}+1\right)^{1/2} + {z_R}^{3/2}\ln\left\{\frac{L}{2z_R}+\left(\frac{L^2}{4{z_R}^2}+1\right)^{1/2}\right\}\right],\end{aligned} \tag{VII.12}$$

where $w_0 = (2z_R/k_1)^{1/2}$ has been used in the last step. We need to find the ${z_R}^{\max}$ value which leads to the maximum filling factor, and minimum $\overline{A}$. However, $\mathrm{d}\overline{A}/\,\mathrm{d}z_R$ is a complicated, so let us find ${z_R}^{\max}$ numerically. From the numerical solution, we obtain the estimated ${z_R}^{\max}$ value, which yields the smallest optical area, as shown in Figure 24.

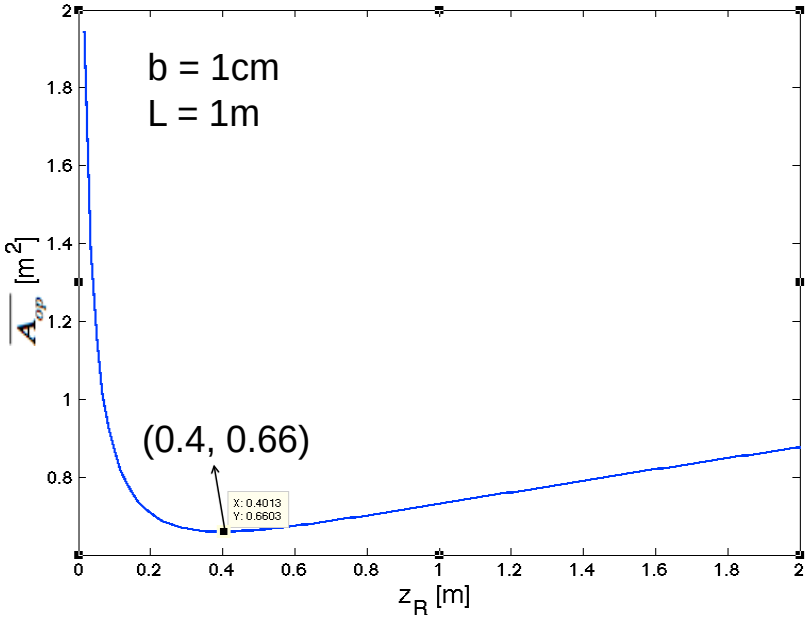

Figure 24. Averaged optical mode area $\overline{A}$ for fundamental Hybrid mode versus Rayleigh length z_R, when $b = 1\text{cm}$ and $L = 1\text{m}$. We see from this graph that $\overline{F_H}^{\max}$ occurs at ${z_R}^{\max} \approx (0.4)L$.

Therefore, the maximum filling factor, $\overline{F_H}^{\max}$, occurs at ${z_R}^{\max} \approx (0.4)L$, giving a peak value of G/jF_H (gain normalized to j and F_H) of about 0.135 and at ${\nu_0}^{\max} \approx 3.85$.

THIS PAGE INTENTIONALLY LEFT BLANK

VIII. CONCLUSION

In this thesis, we have reviewed the basic FEL theory and found solutions of the wave equation for Hermite Gaussian (HG) resonator modes in free space. We have then analyzed the effects of HG modes on FEL theory, including the pendulum equation and gain. We have then studied the Hybrid (HG-Waveguide) resonator modes. There are crucial for long FEL wavelength, where a waveguide must be used in the resonator cavity to prevent the optical beam from diffracting into contact with the undulator. We have analyzed, for the first time, FEL operation with these Hybrid modes.

A waveguide in the resonator cavity produces a change in the FEL resonance parameter. This change has the effect of shifting the gain spectrum away from the traditional (free space) value of resonance. In a fundamental Hybrid mode, the transverse mode area must be used to compute the filling factor, which also affects the gain. We have found a new optimized Rayleigh length, associated with the waveguide, which allows the FEL to have maximum gain. Finally, we recommend the following future work:

- Examine the beam coupling to free space mode outside the Hybrid mode region.
- Examine the output coupling with a partially transmissive mirror versus beam output that using a mirror with a hole.

THIS PAGE INTENTIONALLY LEFT BLANK

LIST OF REFERENCES

[1] W. B. Colson and A. M. Sessler, "Free Electron Lasers," *Annual Review of Nuclear and Particle Science*, vol. 35, pp. 25–54, Dec. 1985.

[2] W. B. Colson, "Free Electron Lasers," Class notes for PH4858, Department of Physics, Naval Postgraduate School, Monterey, CA, fall quarter 2009.

[3] B. Williams, "Higher-Order Modes in Free Electron Lasers," M.S. thesis, Naval Postgraduate School, Monterey, CA, 2005.

[4] A. Kampouridis, "Laguerre-Gaussian Modes in the Free Electron Laser," M.S. thesis, Naval Postgraduate School, Monterey, CA, 2007.

[5] "Free Electron Laser," [Online]. Available: http://en.wikipedia.org/wiki/Free electron laser. [Accessed: Jun. 12, 2010].

[6] R. A. Neuerman, "Simulation and Design Methods for Free Electron Laser Systems," M.S. thesis, Naval Postgraduate School, Monterey, CA, 2009.

[7] "Beam dump," [Online].
Available: http://www-ps.kek.jp/jhf-np/hadronbeam/dump/beamdump.jpg. [Accessed: Oct. 2, 2010].

[8] W. B. Colson, C. Pellegrini and A. Renieri, *Free Electron Laser Handbook*, vol. 6, ch. 5, North-Holland Physics, 1990.

[9] W. B. Colson, "Free Electron Laser Theory," Ph.D. dissertation, Stanford University, Stanford, CA, 1977.

[10] J. D. Jackson, "Invariance of electric charge; Convariance of electrodynamics," in *Classical Electrodynamics*, 3rd ed., Wiley, 1998, pp. 553–558.

[11] R. Vigil, "Hermite-Gaussian Modes and Mirror Distortions in the Free Electron Laser," M.S. thesis, Naval Postgraduate School, Monterey, CA, 2006.

[12] A. E. Siegman, "Wave Optics and Gaussian Beams," in *Lasers*, 1st ed., University Science Books, 1986, pp. 626–662.

[13] H. Kogelnik and T. Li, "Laser Beams and Resonators," *Applied Optics*, vol. 5, no. 10, pp. 1550–1567, Oct. 1966.

[14] F. L. Pedrotti, L. S. Pedrotti, and L. M. Pedrotti, "Characteristics of Laser Beams" in *Introduction to Optics*, 3rd ed., Benjamin Cummings, 2006, pp. 582–606.

[15] M. L. Boas, "Partial Differential Equations," in *Mathematical Methods in the Physical Sciences*, 3rd ed., Wiley, 2005, pp. 619–665.

[16] M. R. Spiegel and J. Liu, "Hermite Polynomials," in *Schaum's Outline of Mathematical Handbook of Formulas and Tables*, 2nd ed., Mcgraw-Hill, 1999, pp. 167–168.

[17] L. R. Elias and J. C. Gallardo, "Cylindrical Gaussian-Hermite Modes in Rectangular Waveguide Resonators," *Applied Physics B*, vol. 31, pp. 229–233, Apr. 1983.

[18] J. J. Degnan, "The Waveguide Laser: A Review," *Applied Physics*, vol. 11, pp. 1–33, Apr. 1976.

[19] R. H. Pantell, "Design and Performance of a Far Infrared, Free-Electron Laser," *Radiation Effects and Defects in Solids*, vol. 122, pp. 571–577, Dec. 1991.

[20] Y. U. Jeong et al., "First lasing of the KAERI compact far-infrared free-electron laser driven by a magnetron-based microtron," *Nuclear Instruments and Methods in Physics Research Section A*, vol. 475, pp. 47–50, Dec. 2001.

[21] J. D. Jackson, "Poynting's Theorem and Conservation of Energy and Momentum for a System of Charged Particles and Electromagnetic Fields," in *Classical Electrodynamics*, 3rd ed., Wiley, 1998, pp. 258–262.

[22] L. R. Elias, G. Ramian, J. Hu, and A. Amir, "Observation of Single-Mode Operation in a Free-Electron Laser," *Physical Review Letters*, vol. 57, no. 9, pp. 424–427, Dec. 1985.

[23] S. Gnanalingam, "Electromagnetic Wave Propagation," Class notes for PH3360, Department of Physics, Naval Postgraduate School, Monterey, CA, winter quarter 2010.

[24] W. B. Colson and P. Elleaume, "Electron Dynamics in Free Electron Laser Resonator Modes," *Applied Physics B*, vol. 29, pp. 101–109, Jun. 1982.

[25] W. B. Colson, "One-Body Electron Dynamics in a Free Electron Laser," *Physics Letters A*, vol. 64, pp. 190–192, Dec. 1977.

[26] Professor W. B. Colson (private communication), 2010.

INITIAL DISTRIBUTION LIST

1. Defense Technical Information Center
   Ft. Belvoir, Virginia
2. Dudley Knox Library
   Naval Postgraduate School
   Monterey, California
3. Chairman, Physics Department
   Naval Postgraduate School
   Monterey, California
4. Professor William Colson
   Naval Postgraduate School
   Monterey, California
5. Professor Robert Armstead
   Naval Postgraduate School
   Monterey, California
6. Professor Joseph Blau
   Naval Postgraduate School
   Monterey, California
7. Headquarter of Army, Library
   Republic of Korea Army
   Gyeryong, Republic of Korea
8. Korea National Defense University, Library
   Goyang, Republic of Korea